Oblikovanje i 3D printanje implantata "skela" od trikalcij-fosfata

Kapo, Faruk

UNIVERSITY OF ZAGREB
FACULTY OF MECHANICAL ENGINEERING AND NAVAL ARCHITECTURE

MASTER'S THESIS

Faruk Kapo

Zagreb, 2016.

UNIVERSITY OF ZAGREB
FACULTY OF MECHANICAL ENGINEERING AND NAVAL ARCHITECTURE

MASTER'S THESIS

Supervisors:

Prof. dr. sc. Tanja Jurčević Lulić
ao.Univ.Prof. Dr. Jürgen Stampfl

Student:

Faruk Kapo

Zagreb, 2016.

I declare that I have written this thesis independently using the knowledge acquired during studies and the listed references.

I have to thank everyone who contributed in any way to making this possible.

I am grateful to ao.Univ.Prof. Dr. Jürgen Stampfl for giving me the opportunity to be a part of the group and work on my thesis at the Vienna University of Technology, specifically at the Institute of Materials Science and Technology. I want to thank Dipl.-Ing.Markus Pfaffinger for all the advice and help during experimental work and creation of this thesis.

I also want to thank prof.dr.sc. Tanja Jurčević Lulić for being my supervisor at University of Zagreb and for supporting the successful completion of this thesis.

I am very grateful to my parents and my sister for all the support, patience and encouragement during my studies.

Faruk Kapo

SVEUČILIŠTE U ZAGREBU

FAKULTET STROJARSTVA I BRODOGRADNJE

Središnje povjerenstvo za završne i diplomske ispite

Povjerenstvo za diplomske ispite studija strojarstva za smjerove:

procesno-energetski, konstrukcijski, brodostrojarski i inženjersko modeliranje i računalne simulacije

Sveučilište u Zagrebu Fakultet strojarstva i brodogradnje	
Datum	Prilog
Klasa:	
Ur.broj:	

DIPLOMSKI ZADATAK

Student: **Faruk Kapo** Mat. br.: 0035180134

Naslov rada na hrvatskom jeziku: **Oblikovanje i 3D printanje implantata „skela“ od trikalcij-fosfata**

Naslov rada na engleskom jeziku: **Designing and 3D Printing of Tissue Scaffolds made of Tricalcium Phosphate**

Opis zadatka:

Tissue engineering for bone regeneration requires the use of porous bone substitute implants, called scaffolds, to serve as template for cell interactions and formation of the extracellular matrix, as well as to provide structural support for the newly formed tissue. Tricalcium Phosphate (TCP) is a biocompatible material especially used for bone scaffolds.

Conventional manufacturing methods for the production of scaffolds, such as gas forming, salt leaching or freeze drying, have the disadvantage of no control over pore distribution, pore size etc. This means there is no repeatability of the micro and macrostructure of the scaffolds. Additive manufacturing (AM) technologies help to overcome this disadvantage. Within AM, stereolithography excels in the achievable surface quality and resolution. Therefore it is the technology of choice to build scaffold structures. The starting material, a colloidal suspension called slurry, consists of organic material and ceramic powder particles. In the current slurry, powder particles settle within a few hours, which means the slurry is not stable and this should be improved.

FEM is a tool for predicting mechanical performance of scaffolds fabricated by AM and thus optimizing their mechanical performance through the intelligent design of their geometry.

Thesis needs to cover the following tasks:

1. Optimization of slurry composition in order to achieve improved stability,
2. Determination of the appropriate processing parameters for the new slurry
   - Adaptation of the printing parameters, cleaning procedure and thermal processing in order to achieve improved printing quality,
3. Designing of different scaffold geometries as 3D lattice of rods based on desirable feature patterns, pore sizes and shapes, and its distribution in the scaffold internal structure,
4. Use of FEM to determine how the different geometrical variables (rod thickness, spacing…) affect the mechanical behaviour of the structure.

Zadatak zadan:	Rok predaje rada:	Predviđeni datumi obrane:
5. svibnja 2016.	7. srpnja 2016.	13., 14. i 15. srpnja 2016.

Zadatak zadao:

Prof.dr.sc. Tanja Jurčević Lulić

Prof. dr. Jürgen Stampfl

Predsjednica Povjerenstva:

Prof. dr. sc. Tanja Jurčević Lulić

TABLE OF CONTENTS

LIST OF FIGURES

LIST OF TABLES

LIST OF SYMBOLS

Symbol	Unit	Description
C_D	nm	cure depth
D_P	nm	penetration depth
d_{50}	μm	ceramic particle size
E	J	energy of the light source
E_C	J	critical energy of the resin
h	μm	interparticle distance
n_{powder}	-	refractive index of the powder
n_{resin}	-	refractive index of the resin
Q	-	light scattering
$V_{scaffold}$	mm^3	volume of scaffold geometry
V_{total}	mm^3	overall volume enclosed by outer edges of the scaffold
λ	nm	light wavelength
ϕ	-	volume fraction of ceramic in a mixture

SAŽETAK

Inženjerstvo tkiva je interdisciplinarno polje koje primjenjuje principe inženjerstva i biologije na razvoj bioloških zamjena koji vraćaju, održavaju i poboljšavaju funkcije tkiva i organa. Cilj inženjerstva tkiva nije zamjena oštećenih tkiva, već njihova regeneracija. U slučaju regeneracije kosti, potrebno je imati trodimenzionalnu i poroznu strukturu koja se naziva skela. Skela mehanički podržava proces regeneracije i olakšava stvaranje novog tkiva. Skela za inženjerstvo tkiva mora ispuniti određene zahtjeve. Osnovni zahtjev je taj da skela bude biokompatibilna, što znači da interakcija između implantata i tijela mora biti povoljna kako ne bi došlo do upale koja bi mogla usporiti ozdravljenje ili uzrokovati odbacivanje implantata. Budući da je skela privremena struktura koju će zamijeniti tkivo, ona mora biti postupno uklonjena. To znači da skela mora biti biorazgradiva kako bi omogućila tkivu da se u potpunosti obnovi. Skela također mora imati mehanička svojstva što sličnija tkivu kojeg zamjenjuje, te mora biti porozna. Dimenzije pora moraju biti nekoliko puta veće od stanica kako bi omogućile ulazak i izlazak hranjivih tvari i otpada, te one moraju biti međusobno povezane.

Biokeramika je pojam koji opisuje biomaterijale koji se proizvode sinteriranjem ili taljenjem anorganskih tvari kako bi se stvorilo amorfno ili kristalno čvrsto tijelo. Trikalcij fosfat je biokompatibilni i biorazgradivi keramički materijal koji ima kemijski sastav sličan sastavu koštanog tkiva. To ga čini idealnim materijalom za upotrebu kao koštanu skelu.

Glavno ograničenje uobičajenih metoda izrade skela je nemogućnost kontroliranja strukturalnih parametara skele. Stoga, upotreba aditivnih tehnologija može pomoći u prevladavanju tog problema. Stereolitografija je aditivna tehnologija proizvodnje koja uključuje polimerizaciju ili skrućivanje tekuće fotoosjetljive smole pomoću svjetlosti, koja opskrbljuje energiju potrebnu za izazivanje polimerizacije.

3D printanje keramike je proces koji se sastoji od 2 koraka. Prvi korak je izrada „zelenog dijela“ koristeći stereolitografiju, pri čemu skrućeni polimer služi kao vezivo koje drži keramičke čestice na okupu. Drugi korak je termička obrada koja se sastoji od uklanjanja veziva i sinteriranja, pri čemu se dobiva konačni proizvod. Tijekom termičke obrade dolazi do povećanja tlaka unutar strukture zbog izgaranja polimera. Kako bi se izbjegla oštećenja strukture zbog previsokog tlaka, potrebno je koristiti točno određenu brzinu zagrijavanja.

Na Tehničkom Sveučilištu u Beču je razvijena nova vrsta 3D printera koji se nazivaju *Blueprinter*. Zasnivaju se na DLP (Digital Light Processing) tehnologiji koja omogućava selektivno skrućivanje fotoosjetljive smole. Sustav koristi LED valne duljine 460 nm kao izvor svjetlosti i DMD (Digital Micromirror Device) čip kako bi projicirao slike pojedinih slojeva na ravninu gradnje. Rezolucija DMD čipa je do 1920x1200 piksela, a debljina jednog sloja može biti podešena između 15 i 75 μm.

Polazni materijal koji se koristi za stereolitografiju keramičkih materijala je koloidna suspenzija koja se naziva slurry. Sastoji se od čestica keramičkog praha koje su dispergirane u organskoj tvari. Sastojci slurrya su: monomeri, otapalo, fotoinicijator, disperzirajuće sredstvo, apsorber svjetla te keramički prah. Problem sa slurry-em je da je njegova dugotrajna stabilnost vrlo slaba, jer se javlja sedimentacija u roku od nekoliko sati. Kada je slurry nestabilan, potrebno ga je promiješati prije svake upotrebe. Dodatni nedostatak lošije stabilnosti je njegov negativan učinak na 3D printanje. Stoga, bilo je potrebno provesti optimizaciju slurry-a s ciljem poboljšanja stabilnosti. Osnovna ideja za poboljšanje stabilnosti je uvođenje voska u mješavinu umjesto otapala. Njihova uloga je jednaka pri termičkoj obradi, a razlika je u tome što je vosak na sobnoj temperaturi u krutom stanju.

U ovom radu testiran je utjecaj promjene komponenti i njihove količine na stabilnost te kvalitetu printanja slurry-a. Provedeni su testovi stabilnosti na sobnoj i povišenoj temperaturi te testovi 3D ispisa s različitim sastavima slurry-a. Variranjem monomera, disperzirajućeg sredstva i otapala, te s dodatkom voska, dobivena su različita svojstva slurry-a, te je u konačnici određen sastav kojim je postignut stabilan slurry. Osim toga, određeni su odgovarajući parametri za 3D ispis s novim slurry-em, te je povećana kvaliteta printanja. Također, određen je i prikladan postupak čišćenja „zelenog dijela“ od preostalog slurry-a nakon printanja.

Nakon što je razvijen materijal pomoću kojeg je uz korištenje aditivnih tehnologija moguće izrađivati skele, potrebno je prije same izrade i upotrebe optimizirati njihov mehanički odziv. Predviđanje njihovog ponašanja pri opterećenju je moguće postići upotrebom FEM alata. Poroznost je osnovna varijabla dizajna za koju je poznato da utječe na obnovu tkiva. U ovom radu su oblikovane dvije vrste skela kojima je varirana poroznost (55% i 80%). Promjena poroznosti je dobivena variranjem parametara skele kao što su razmak pora i veličina pora. Jedna vrsta skele je imala pravokutne pore, dok se druga sastojala od naslaganih šipki. Simulirano je tlačno opterećenje skela tako što je na gornju površinu zadan pomak u vertikalnom smjeru. Rezultati su pokazali da je raspodjela naprezanja povoljnija pri manjoj

poroznosti. Također, kod skele s pravokutnim porama vidljiv je manji utjecaj poroznosti na naprezanja, ali su moguće koncentracije naprezanja u rubovima pora. Prilikom dizajniranja skele potrebno je napraviti kompromis između mehaničkog ponašanja skele i cjelokupne poroznosti kako bi se dobila odgovarajuća svojstva.

Ključne riječi: koštana skela, trikalcij fosfat, stereolitografija, stabilnost mješavine, oblikovanje skele, FEM analiza

SUMMARY

The aim of tissue engineering is to regenerate damaged tissues, instead of replacing them. In case of bone regeneration, it is required to have a three-dimensional and porous architecture called a scaffold, which mechanically supports the regeneration process and facilitates the formation of new tissue. Tricalcium phosphate is a biocompatible and biodegradable ceramic material with chemical composition similar to the bone tissue. This makes it the ideal material for the use as a bone scaffold. The lack of control over scaffold architectural parameters is the main limitation of the conventional fabrication methods. Therefore, additive manufacturing can help to overcome this issue. Stereolithography is an additive manufacturing technology, which involves the polymerization or solidification of a liquid photosensitive polymer through the use of an irradiation light source, which supplies the energy that is needed to induce polymerization. The starting material used for stereolithography of ceramic materials is a colloidal suspension called slurry. It consists of ceramic powder particles dispersed in organic material. The issue with the slurry is that its long time stability is very poor, as sedimentation occurs within a few hours. When the slurry is unstable, it has to be mixed every time before it is used. Another downside of poor stability is its negative effect on the printing. Therefore, optimization of the slurry was necessary. Stability and printing tests with different slurry formulations were carried out. By varying monomers, dispersing agents and solvents, and with the addition of wax, a stable slurry was achieved. Additionally, printing parameters for the new slurry have been determined and the printing quality was increased.

Key words: bone scaffold, tricalcium phosphate, stereolithography, slurry stability, scaffold design, FEM analysis

1. INTRODUCTION

1.1. Tissue engineering

Disease, injury and trauma can lead to damage and degeneration of tissues in the human body, which necessitates treatments to help their repair, replacement or regeneration [1]. The usual treatments are focused on transplanting tissue from one site to another in the same patient (an autograft) or from one individual to another (a transplant or allograft) [1]. While these methods have proven to be lifesaving, there are also problems with both techniques. Collecting autografts is expensive, painful and constrained by anatomical limitations. Allografts and transplants carry risks of rejection by the patient's immune system, as well as possible infection from the donor. Also, there is a problem with accessing enough tissue for all the patients.

The aim of tissue engineering (TE) is to regenerate damaged tissues, instead of replacing them. Tissue engineering has been defined as an interdisciplinary field that integrates principles of engineering and life sciences to develop biological substitutes that restore, maintain, or improve tissue function [2, 3]. It can also be defined as the use of a combination of cells, engineering materials, and suitable biochemical factors to improve or replace biological functions in an effort to affect the advancement of medicine [3].

The approach of tissue engineering is different compared to current treatments, which focus mainly on drugs to encourage the body to fight diseases. In tissue engineering, a highly porous artificial extracellular matrix (ECM) or scaffold is used to enable cellular growth and tissue regeneration.

Three main strategies are commonly used in tissue engineering: infusion of isolated cells, treatment with tissue-inducing growth factors, and implantation of scaffolds with or without the tissue-specific cells and growth factors [4].

Great advancements were made over the past two decades due to more knowledge being gained in biology, clinical sciences, physical sciences and technology, and more collaboration between clinicians, engineers and scientists.

1.2. Scaffolds for bone tissue engineering

In case of bone regeneration, it is required to have a three-dimensional and porous architecture called a scaffold. In addition to supporting bone-forming cell proliferation, migration and mineralization, scaffold also mechanically supports the bone tissue regeneration process [4]. Scaffolds are also designed to have interconnected porosity that allows ingrowth of cells, tissue infiltration and eventually, new bone tissue formation [4].

Scaffolds play a critical role in tissue engineering. The function of scaffolds is to direct the growth of cells either seeded within the porous structure of the scaffold or migrating from surrounding tissue [5]. Scaffolds should be designed to provide a structural framework as well as a microenvironment for the cells and to facilitate the formation of new tissues [6].

Scaffolds serve numerous functions critical for the success of tissue regeneration, which include [7]:

- Serving as space-holders to prevent intrusion of tissues from the surrounding area into the affected site.
- Providing a temporary support structure for the tissue that they are intended to replace.
- Creating a substrate for cells to attach, grow, proliferate, migrate, and differentiate on.
- Serving as a delivery vehicle for cells, facilitating their retention and distribution in the region where new tissue growth is desired.
- Providing space for vascularization, new tissue formation, and remodelling to occur.
- Enabling the efficient transport of nutrients, growth factors, blood vessels, and removal of waste material.

In order to achieve all the required functions, scaffold has to meet certain requirements. These requirements are summarized in Table 1 and explained below.

Table 1. Scaffold design criteria [4]

Scaffold design criteria	Resulting function in engineered tissue
Biologic compatibility	Non-toxic/minimal inflammatory response
3D matrix architecture	Physiologically relevant environment for cell function
Void space	Highly porous and interconnected pores to allow cell infiltration, transport of nutrients, humoral factors and waste products
Surface chemistry and topography	Cell attachment and cell-matrix interactions
Appropriate mechanical behavior	Seamless integration with surrounding tissue(s) able to withstand in vivo forces and avoid stress shielding
Degradation rate	Scaffold lead to the formation of a functionalized matrix
Structural anisotropy	Anisotropic mechanical behaviour Influence orientation of cells and ECM deposition

The main requirement of any scaffold for tissue engineering is that it must be biocompatible. The scaffold is required to cause an appropriate immune response from the host tissue on implantation. It means that the interactions between the scaffold and host tissue should be favourable, in order to avoid causing a severe inflammatory response which might reduce healing or cause rejection by the body [1, 7]. It is also necessary for the scaffold to be biofunctional, which means that the material should support and promote cell attachment and function, as well as cell-material interactions [7, 8].

Since scaffolds act as temporary structures that are eventually replaced by native tissue, they need to be gradually removed from the implant site. Therefore, they must be biodegradable in order to allow cells to produce their own extracellular matrix (ECM) [7, 1]. Biodegradability indicates the ability of the material to be degraded by biological elements into non-toxic products, leaving behind the desired living tissue [8]. The by-products of this degradation should be able to exit the body without interference with other organs [1]. Furthermore, it is extremely important to have matching rates of degradation of scaffold and regrowth of new tissue. This requirement is very difficult to achieve. The scaffold should gradually transfer the function of load-bearing and support to the newly growing tissue [7]. If the scaffold degrades at a very fast rate, the new tissue will be suddenly exposed to greater forces than what it can endure, as it will not have had enough time to become capable of bearing the new forces and can therefore be negatively affected. On the other hand, if the scaffold degrades at a very slow rate, it can result in stress shielding of the growing tissue, thereby protecting it from the forces and making it more prone to injury later on [7].

The scaffold should have mechanical properties that match those of the host tissue as closely as possible [1, 7]. It is necessary in order to prevent tissue healing from being compromised by mechanical failure of the scaffold before the new tissue generation occurs [7]. Scaffold must also be strong enough to allow surgical handling during implantation [1]. For bone tissues, the implanted scaffold must have sufficient mechanical integrity to function from the time of implantation to the completion of the bone remodelling process [1].

Another important requirement for scaffolds used in TE is their architecture. Scaffold architecture mainly dictates the transport that occurs within it. The transport consists of delivery of oxygen and other nutrients, removal of waste, transport of proteins and cell migration [7]. A scaffold cannot be completely solid as cells need to grow within it and they need to be supplied with nutrients [7]. Therefore, the scaffold needs to have holes or pores. The pore size should at least be a few times the size of the cells to provide enough space for the entry and exit of nutrients and waste [7]. There is no common pore size range that is suitable for all types of tissue growth as cells of different tissues have different dimensions [7]. Porosity is the amount of void space within the scaffold structure. Scaffolds need to possess high porosity and high surface area-to-mass ratio for promoting uniform cell delivery and tissue ingrowth as well as have an open pore network for optimal diffusion of nutrients and waste [7]. Scaffold porosity is related to the physical and mechanical properties of the scaffold. A more solid and less porous scaffold could result in better mechanical properties. Increasing the porosity can thus compromise the mechanical integrity of the scaffold. Therefore, it is needed to optimize scaffolds based on their specific mechanical requirements balanced with their desired diffusion characteristics [7]. It is not sufficient for a scaffold to be porous. The pores in the scaffold need to be interconnected for efficient delivery of nutrients to the interior and removal of waste to the exterior of the scaffold. Pore interconnectivity is also important for cell migration and tissue ingrowth [7].

The local chemical environment controls the interactions between cells and scaffolds that occur at the surface [7]. Scaffold should have the desired surface properties to enable cell attachment, growth and differentiation as well as extracellular matrix formation [7]. The adhesion and growth of different types of cells depend on surface characteristics such as chemistry, charge, roughness, and rigidity [5].

The scaffold should be easily processed into three-dimensional complex shapes in a well-controlled and reproducible manner [1]. It should be cost effective, in order to become

clinically and commercially viable [7]. Another important factor is determining how a product will be delivered and made available to the clinician, and also how it will be stored [1].

1.2.1. Bioceramic scaffolds

Bioceramic is a term describing biomaterials that are produced by sintering or melting inorganic raw materials to create an amorphous or a crystalline solid body. They can be used in medical and dental applications as implants and replacements. Bioceramic materials show promise in meeting the previously mentioned requirements.

The components of ceramics include calcium, silica, phosphorous, magnesium, potassium, sodium, zirconium, aluminium and many others [3]. Materials that are classified as bioceramics include alumina, zirconia, calcium phosphates, silica-based glasses or glass ceramics and pyrolytic carbons. Bioceramics are biocompatible and can be inert, bioactive and degradable in physiological environments, which makes them the ideal biomaterial [9].

Calcium phosphates bioceramics are very promising materials in producing bone substitute components, as the degradation of these ceramics produces calcium and phosphate ions, which regulate bone metabolism, as they promote new bone formation through osteoinduction [10]. They have good biocompatibility and osteoconductive properties, as well as the capability to integrate into bone structures and support bone ingrowth [4]. Calcium phosphate materials are one of the few biomaterials that have chemical composition similar to the bone tissue [11].

There is a range of calcium phosphate ceramics, depending on the molar ratio of calcium and phosphate, with different biodegradation properties [10]. The most frequently used calcium phosphates are β-tricalcium phosphate (β-TCP), hydroxyapatite (HA), tetracalcium phosphate (TTCP) and its derivatives and their combinations, for instance biphasic calcium phosphate (BCP), which is a mixture of TCP and HA [12, 13]. The rate of biodegradation of calcium phosphates increases in the following order: HA < β-TCP < α-TCP < TTCP [12].

Calcium phosphate-based biomaterials and bioceramics are now used in a number of different applications throughout the body, covering all areas of the skeleton [13]. Depending upon which properties are desired, different calcium phosphates can be used.

Unlike metals and polymers, ceramics are difficult to shear plastically due to the ionic nature of the bonding. Therefore, ceramics have low ductility and high resistance to deformation [14, 4]. Ceramics are very susceptible to cracks because instead of undergoing plastic deformation

they will fracture elastically on initiation of a crack. Ceramics have low tensile strength compared to compressive strength [14].

1.2.2. Tricalcium phosphate (TCP)

Tricalcium phosphate (TCP) can be defined as a bioceramic with bioresorbable properties [4]. TCP is generally produced in three allotropic forms, β-TCP, α-TCP, and α'-TCP, which differ in crystalline structure and mechanical properties. Chemical formula of TCP is: $Ca_3(PO_4)_2$. The β-TCP formulation is appropriate for bone scaffolding due to the biological response and mechanical properties of this allotropic phase [10]. When implanted, TCP implants provide an ideal environment for cellular reaction and colonization by osteoblasts. This leads to osteoconduction in which bone grows on and bonds to the implant, promoting a functional interface [13]. The main reason behind the use of β-TCP as bone substitute material is its chemical similarity to the mineral component of bone and teeth [13]. Unfortunately, TCP exhibits relatively poor tensile and shear properties. The mechanical properties of TCP are generally inadequate for many load-bearing applications (3 MPa – 5 MPa), therefore its use is restricted to non-load bearing defects or pure compression loading [13].

1.3. Scaffold fabrication

The formation of a porous structure is the main goal of scaffold fabrication. However, the size, shape and the interconnectivity of the pores are crucial aspects to ensure rapid vascularization and growth of the surrounding bone into the scaffold. Several methods have been developed to create highly porous scaffolds, including fiber bonding, solvent casting/particulate leaching, melt molding, extrusion, gas foaming, freeze drying and phase separation [12]. These are conventional technologies as they have been used commonly in chemical engineering, ceramic engineering, metal production and forming, composite technology and other fields for purposes other than biomedical applications or for producing porous structures that are not intended for the biomedical industry. Because of the relative ease in using these technologies, they are still commonly used to produce various scaffolds for the regeneration of tissues or organs [7, 6].

The choice of manufacturing method can influence different characteristics of the scaffold, including structural architecture, mechanical properties, biocompatibility, and biochemical properties. Some methods, such as freeze-drying, can generate porous scaffolds containing both small (15 to 35 μm) and large (>200 μm) pore sizes. Using these conventional

techniques, scaffold properties can only be controlled by process and equipment parameters rather than design parameters [15]. Therefore, a core limitation of these technologies is the lack of precise control over scaffold architectural parameters such as pore size, shape, distribution, and interconnectivity as well as the overall scaffold shape [7]. Extensive use of highly toxic solvents and extreme processing conditions (high temperature, pressure) in most of the current fabrication methods are disadvantages for advanced designs and strategies [15]. An adequate pore size and a uniformly distributed and interconnected pore structure that allow easy distribution of cells throughout the scaffold structure are very important [3].

1.3.1. Additive manufacturing

The fabrication of hierarchical porous structures, which consist of both a microscopic pore structure and a macroscopic pore structure, is more easily accomplished using additive manufacturing technologies (AM). These techniques have overcome certain problems faced in traditional methods and allow the reproducible fabrication of scaffolds with complex architecture directly from a computer-aided design (CAD) file [7, 12]. Generated 3D CAD data are processed and sliced into layers of equal thickness, each of which is the cross-section of the 3D model at a certain level. Sliced data are imported into the AM system to fabricate 3D objects layer-by-layer. In this fabrication process, layers are built vertically and fused to form the final physical object [10]. The ability to translate an electronic data set into a scaffold opens up the possibility for patient-specific scaffolds based on computed tomography (CT) or MRI data [7].

Based on their working principles, the existing AM systems can mainly be categorized into three groups: (1) powder-fusion-based techniques; (2) particle- or cell-deposition-based techniques; and (3) photo-polymerization-based techniques [10]. The examples of available AM techniques are stereolithography apparatus (SLA), selective laser sintering (SLS), laminated object manufacturing (LOM), fused deposition modeling (FDM), and three dimensional printing (3DP) [12].

1.4. Stereolithography

Stereolithography (SLA) was developed by Chuck Hull in 1986 at 3D Systems and it was the first commercialized rapid prototyping method (Figure 1) [16]. This technique involves the polymerization of liquid monomers from exposure to ultraviolet radiation [17]. It produces parts one layer at a time by curing a photoreactive resin with a UV laser or another similar

power source [10]. There are several different approaches to SLA, including direct/laser writing and mask-based writing [16]. Components for the direct/laser writing include a movable platform, a tank of liquid resin, a UV light beam, and a computer interface. The mask-based writing contains the movable platform, resin vat, computer, and UV beam. It also includes a digital micromirror device (DMD), which serves as a mask that allows for the curing of a single layer at once. When the resin is exposed to the UV light, it cures (solidifies) according to the exposed pattern and adheres to the layer produced before it [18].

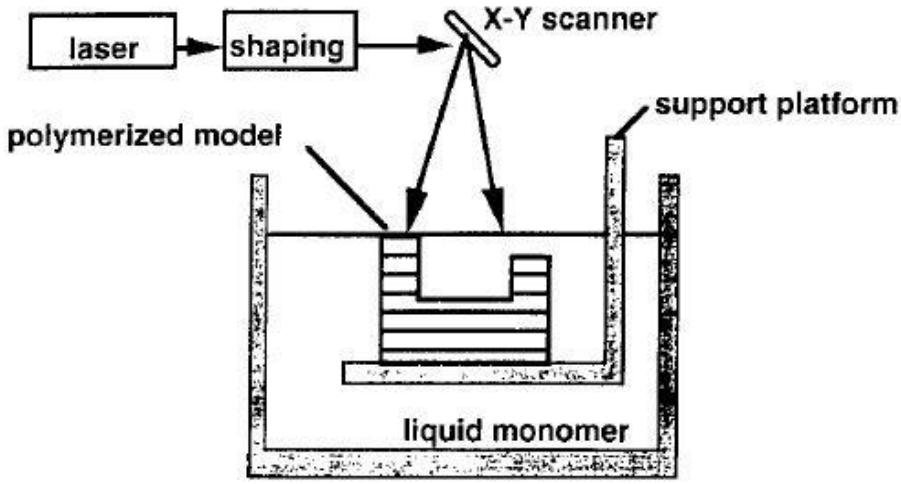

Figure 1. Schematic of the stereolithography apparatus [17]

The direct laser writing method is able to generate detailed 3D objects, but it is also time-consuming. The mask-based method uses the DMD where millions of mirrors can be simultaneously controlled. It allows an entire layer to be cured at once, greatly reducing layer production time [16]. The writing methods are shown in Figure 2.

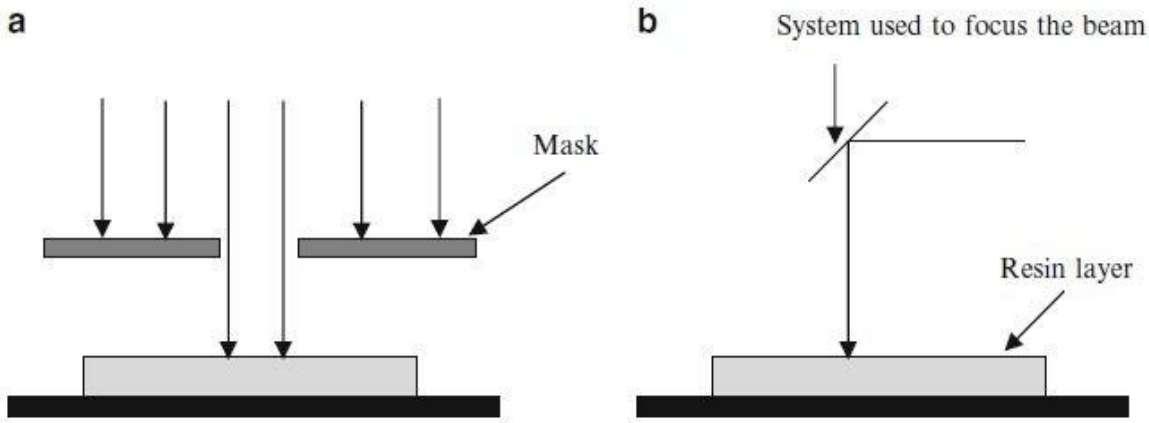

Figure 2. Writing methods in stereolithography; mask-based method (a), direct/laser writing (b) [19]

Resins are one of the main limitations of SLA. It is not only due to the cost associated with the resin but also due to the fact that only one resin can be used in the printing process at a time, thus limiting overall device design [16]. Resins usually have either epoxy or acrylic bases, and the majority of these materials are brittle and can shrink upon polymerization.

The thickness of the cured layer (C_D) can be expressed by the following equation:

$$C_D = D_P \ln\left(\frac{E}{E_C}\right), \tag{1}$$

where C_D is the cure depth, E is the energy of the light source, E_C represents a "critical" energy of the resin, and D_P is the penetration depth of the light into the resin [20]. Penetration depth can be obtained with the following equation:

$$D_P = \frac{2}{3} \cdot \frac{d_{50}}{Q \cdot \phi}, \tag{2}$$

where:

$$Q = \frac{h}{\lambda} \cdot \left(n_{powder} - n_{resin}\right)^2 \tag{3}$$

In the equations (2) and (3), d_{50} is the ceramic particle size, Q is a term for scattering, ϕ is the volume fraction of ceramic, h is the interparticle distance, λ is the wavelength of the light, while n_{powder} and n_{resin} are refractive indexes of the powder and the resin [17].

1.4.1. Stereolithography of ceramic materials

The starting material used for stereolithography of ceramic materials is a colloidal suspension called slurry. It consists of ceramic powder particles dispersed in organic material (UV-curable resin).

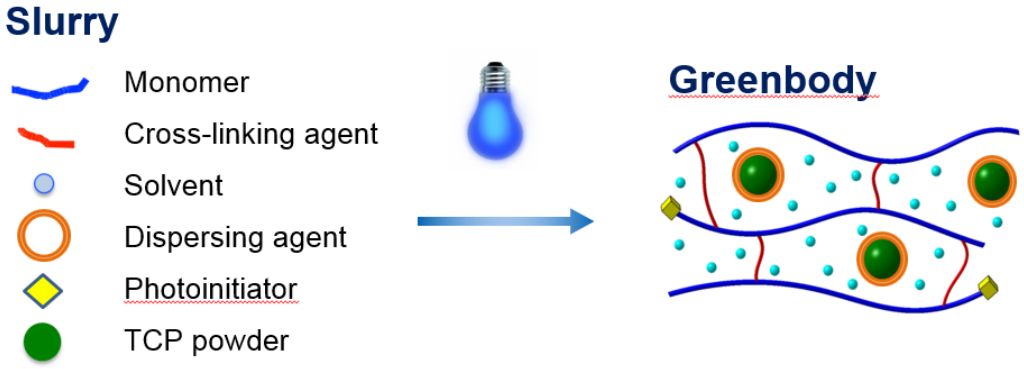

Figure 3. Creation of the green part [21]

3D-printing of ceramics is a two step process that consists of stereolithography and a thermal treatment. It involves building the structure called „green part“ using stereolithography methods (Figure 3). The UV cured polymer acts as the binder to hold the ceramic particles together before the thermal treatment. The green part is then subjected to binder removal through an appropriate thermal treatment (debinding and sintering), that ensures the final properties of the model (Figure 4). During debinding, organic matrix is burned out, while during sintering a dense ceramic part is obtained [23].

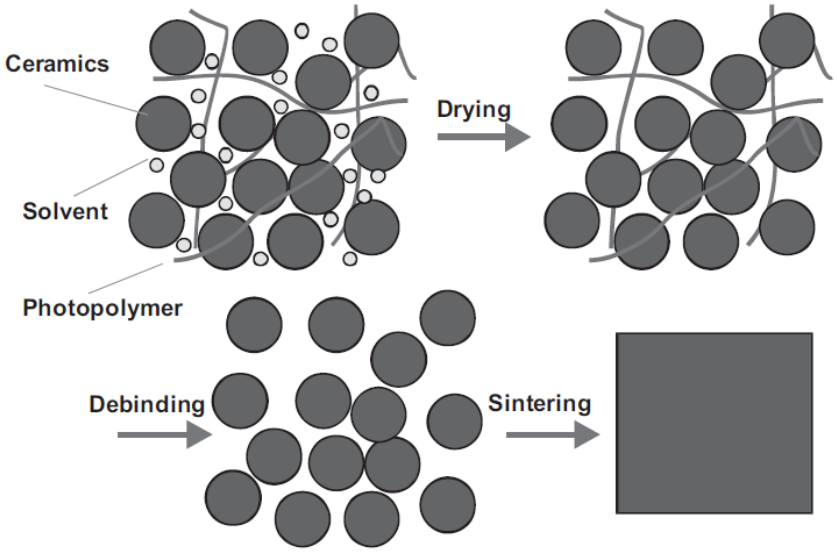

Figure 4. Steps of the thermal treatment [22]

When using a constant heating rate during debinding, the resulting internal gas pressure varies based on different degradation temperatures of the used components [23]. If the gas pressure becomes too high, it could damage the structure of the green part. Therefore, a specific degradation rate of the organics must not be exceeded. This can be controlled by the relative weight loss of the green part during debinding. By adjusting the heating rates and isothermal plateaus, an approximately constant weight loss rate can be achieved [23]. The composition of the organic part also influences the debinding process. Temperature zones of high outgassing and diffusion activity are influenced by the cross-linking density and the double bond rate of the green part [23]. The success of the debinding process is influenced by the characteristics of the used ceramic powder, specifically particle geometry and size distribution. Small powder diameter (d_{50}< 1μm) significantly increases the risk of intralaminar cracks during the debinding process [23]. This could be because of limited diffusion of the gases. The solution

to this problem could be increasing the duration of the debinding process. TCP, with its larger particles (1 μm – 20 μm) allows a much easier debinding process [23].

The burn-out of all organic substances leads to a loss in weight, as well as a dimensional shrinkage (Figure 5). The theoretical weight loss should be equivalent to the amount of used organic substances in the slurry. However, as demonstrated in [23], the actual weight loss is higher than expected. The reason for this could be the hygroscopic property of the slurry. The humidity of the surrounding air leads to absorbtion of water in the slurry during the building process, as well as during the time of storage [23].

Figure 5. Comparison of green part (left) and sintered part (right)

The extent of shrinkage depends on the solid loading of the slurry. As shown in [23], the higher the solid loading the lower the shrinkage. Therefore, the aim is to achieve solid loading as high as possible. If the dimension changes are reduced, there is also an increased accuracy concerning the shape after the thermal treatment [23]. A high solid loading provides an easier debinding process as there is less organic material to burn out.

The success of the debinding process always increases with an increase of the surface-to-volume ratio of a given 3D structure [23]. Therefore, the debinding of porous structures is easier compared to parts with larger wall thickness. Smaller parts are always easier to debind than larger ones while spheres are the most difficult structures for debinding [23].

Because of these observations, it is necessary to optimize the debinding process for specific geometries as well as for the type of ceramic powder and the used organic components [23]. Before the optimization, in order to obtain more information about the evaporation of the solvent and the pyrolysis of other organic components, green parts are subjected to thermal analysis [22].

1.5. Photopolymerization

A polymerization reaction consists of adding many monomer units M to each other, thereby creating a macromolecule [24]. The polymerization process consists of these steps: photoinitiation, chain propagation and termination [25]. The basic scheme of the reaction is:

$$M \rightarrow M{-}M \rightarrow\rightarrow (M)_n \tag{4}$$

In the equation (4), M is the monomer or oligomer unit, and M_n is the macromolecule containing *n* monomer units. The initiation step of this reaction is the decomposition of an initiator molecule I. This produces an initiating species (for instance, a free radical R*), that reacts with the first monomer unit (Figure 6). This reaction produces monomer radicals, which combine with new monomers. Monomer radicals expand in a chain reaction, until two radicals meet with each other [25].

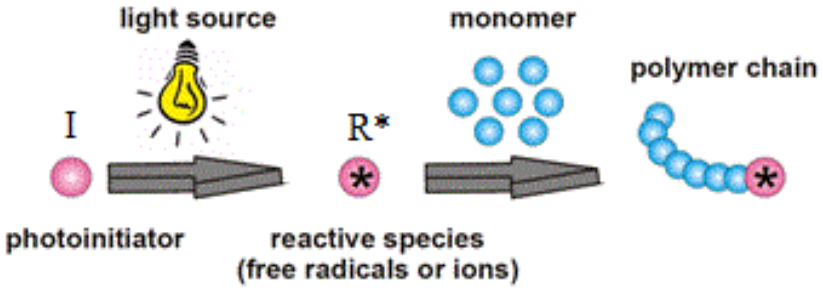

Figure 6. Photopolymerization [26]

Different methods for activation of the polymerization are available, such as heat, light, electron beam, X-rays, γ-rays, plasma, microwaves and pressure [24]. Photopolymerization refers to the process of using light as an energy source which results in the formation of a polymer. Light induces the conversion of small molecules in the liquid state to solid, insoluble macromolecules [25]. A photopolymerizable formulation consists of a monomer/oligomer matrix, a photoinitiator and various additives, for instance wetting, dispersing agents and pigments according to the applications [24].

A monomer is a rather small molecule having usually one or several chemical reactive functions, while an oligomer is a large molecular structure consisting of repetitive units of a given chemical structure that constitutes the backbone and containing one or more reactive chemical functions [24]. Monomers or oligomers are usually not sensitive to the available lights. Therefore, the addition of a photoinitiator (PI) is necessary. When the photoinitiator is exposed to the light, an initiating species is produced [24]. Photoinitiators can be classified

according to the wavelength range of the light used for their activation or according to the mechanism employed for the production of initiating species. The types of light most frequently used for photopolymerization are medium-wave ultraviolet light (UVB, 280 – 315 nm), long-wave ultraviolet light (UVA, 315 – 380 nm), visible light (VL, 400-780 nm) and short-wave infrared light (NIR, 780 – 1500 nm) [27]. Therefore, we differentiate between UV, VL and NIR photoinitiators, which absorb light in the respective spectral region. Depending on the starting molecule, initiating species can be of different nature: radical (R*), cationic (C+), and anionic (A−) [24]. Accordingly, the usual types of photopolymerization reactions can occur: radical, cationic, and anionic photopolymerization. A good photoinitiator should be easily reduced to an initiating species upon light irradiation and provide radicals or cations active enough to react with monomers or oligomers [25].

When using multifunctional monomers or oligomers, the photoinduced polymerization reaction develops in the three directions of space, and it also leads to a cross-linking reaction, thereby creating a polymer network [24]. Sometimes, the reaction is described as a cross-linking photopolymerization.

1.6. Blueprinter

At the Vienna University of Technology, Institute of Materials Science and Technology, a new kind of 3D-printers, called Blueprinters were developed [23]. They are based on Digital Light Processing (DLP) technology, which allows the selective curing of a powder filled photosensitive resin [28]. The exposure of each layer takes place from below through the transparent vat. Vat is a reservoir which contains the printing material. This technology uses high performance LED as a light source and a digital micromirror device chip (DMD) as dynamic mask to project images of each layer onto the building plane [28]. By using dynamic masks the entire cross section of the part is cured at once, which leads to a significant higher building speed [22]. The resolution of the DMD chip is up to 1920x1200 pixels, while specially designed optical system leads to pixel sizes between 25 and 60 μm [23]. The LED emits light with the wavelength of 460nm (blue light) and the light intensity at the vat is up to 100 mW/cm^2 [22, 23]. Layer thickness can be set between 15 and 75 μm [22].

In addition to the light engine, Blueprinter components include a linear axis, a tilting mechanism, a rotating mechanism, a building platform with integrated back light device, heating system and the coating system [22]. By using the coating system, it is possible to process highly viscous ceramic slurries [29]. Also, a very small amount of material is needed

to start the process [22]. The heating system can keep the temperature of the vat, and therefore also the slurry, at an elevated temperature, allowing the use of the slurry components with higher melting point. Figure 7 shows the principle of the Blueprinter.

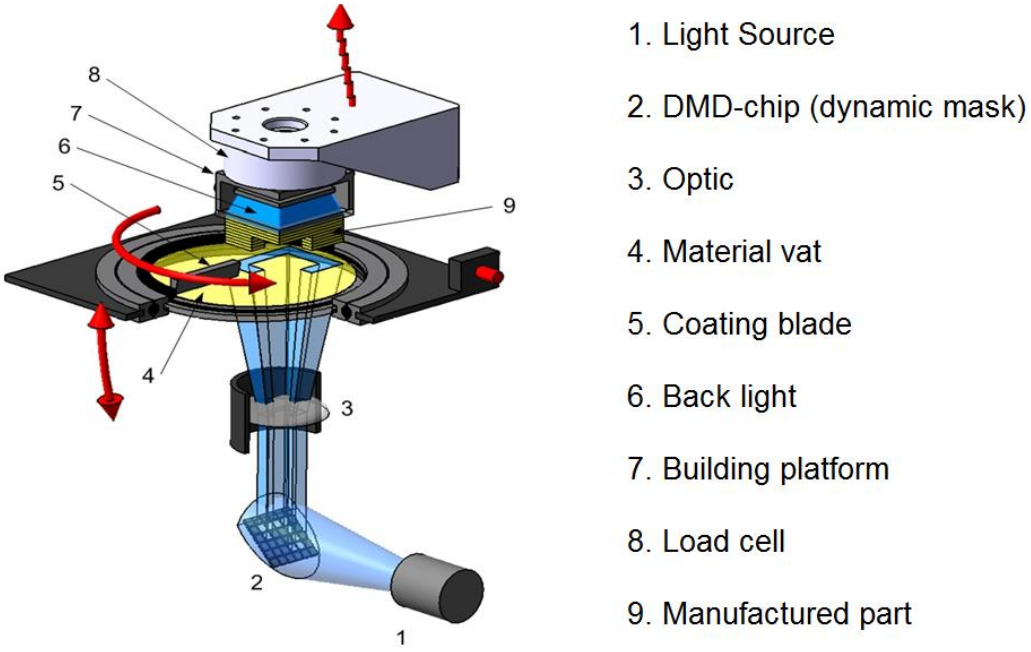

Figure 7. Principle of the Blueprinter [23]

One layer of the part is created as follows. Coating blade moves from one side of the vat to the other, leaving a thin layer of fresh material on the vat. The building platform is then lowered towards the vat, leaving a specified gap, depending on the chosen layer thickness. The light engine then projects the image of the corresponding cross section. The exposed parts of the resin solidify and create a polymer network. The vat is then tilted away from the building platform while the building platform (together with the cured parts) is raised to the previous position to allow the blade to recoat the vat. The process is then repeated for the next layer. Repeating these steps enables the top-down printing of green bodies of nearly every geometry imaginable, including pores or hollow spaces and even over-hangings to a certain limit [28].

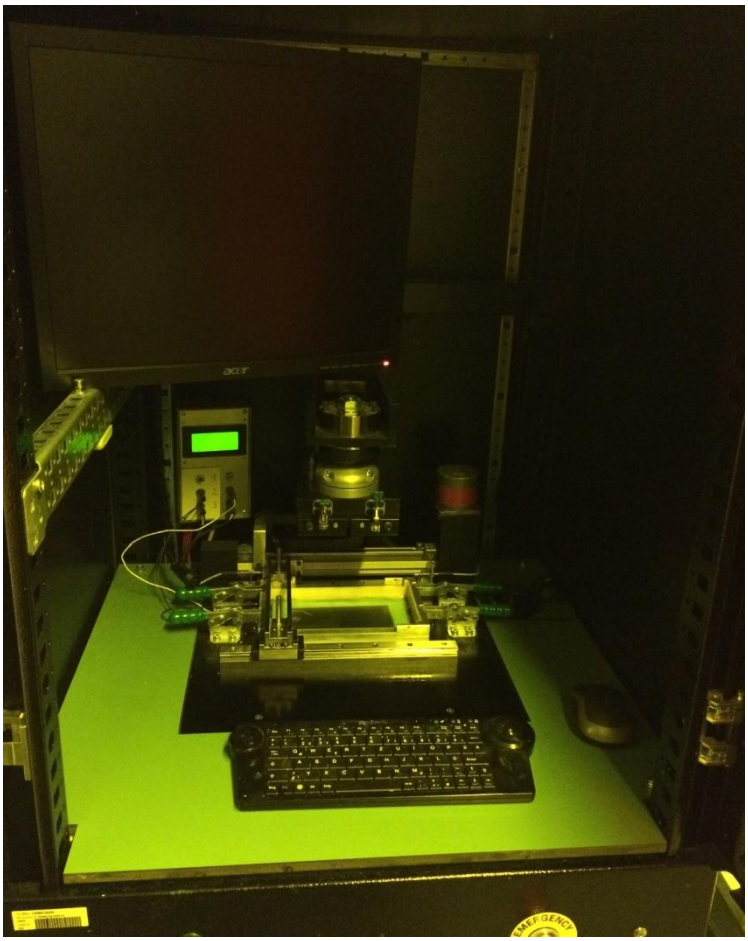

Figure 8. Blueprinter 6

1.7. Starting material – slurry

Candidate ceramic slurry for stereolithography must satisfy several requirements [17]. In order to avoid deformation and cracking during binder removal, to reduce the shrinkage during sintering, and to obtain homogeneous and dense ceramic parts after sintering, it is necessary to minimize the organic concentration in the suspension. Therefore, a high solid loading (volume percentage of ceramic powder in the slurry) is necessary. However, the viscosity of the suspension must be as low as possible to allow a good recoat of the vat [30]. For the successful processing of ceramic slurries with the presented DLP system, a maximum viscosity of approximately 20 Pa s is allowed [22].

Slurries for stereolithography of ceramic materials contain at least one polymerizable liquid organic component, a solvent, a photoinitiator, light absorber, dispersing agent and an inorganic phase in form of ceramic powder [28].

Monomers with different functionality and molecular weight can be used. Due to their fast curing, the most commonly used polymerizable components are acrylate and methacrylate monomers [19]. Acrylate is activated by a photoinitiated radical which binds itself to the acrylate and breaks the double bond [25]. This enables another acrylate to bind to the structure and the chain reaction can propagate. The viscosity of the monomers is also important as it influences the final slurry viscosity [17].

Solvents which are added into the mixture influence the viscosity of the slurry. They are also important during thermal treatment because the solvent is the first component to evaporate. Therefore, an open porosity is created inside the structure of the green part. This facilitates the diffusion and evaporation of the pyrolyzed polymer components afterwards [23].

Dispersing agent influences the slurry viscosity, but its main role is to enable dispersion of ceramic particles in the organic medium, preventing the formatiom of agglomerates and allowing a good homogeneity [31]. It can also be useful in allowing a higher solid loading to be achieved, while keeping the viscosity under the required limits.

A photoinitiator is a compound especially added to a formulation to convert absorbed light energy into chemical energy in the form of initiating species (free radicals or cations) [32]. The excited free radicals combine and react with the monomer molecules (M) to form larger reactive molecules. These reactive molecules continue to react with adjacent monomers to form longer polymeric molecules. The polymeric molecules keep growing until two of them combine and terminate the reaction. The solidified polymer structure forms by the entanglement and cross-linking of these polymer chains [33].

It is necessary to add a specific amount of a light absorber into the slurry, as it minimizes light scattering (limits the spreading of polymerization) and therefore improves printing accuracy. Light absorber reduces penetration and curing depth while increasing the required energy [33].

As the inorganic phase, bioceramic materials are used. They are biocompatible and can be inert, bioactive and degradable in physiological environments, which makes them the ideal biomaterial [9]. Calcium phosphate bioceramics are important for hard tissue repair because of their similarity to the minerals in natural bone, and their excellent biocompatibility and bioactivity [13].

1.8. Colloidal suspension

Colloidal system or colloidal dispersion is a heterogeneous system which is made up of dispersed phase and dispersion medium [34]. In colloidal dispersion one substance is dispersed as very fine particles in another substance.

Dispersed phase and dispersion medium can be solid, liquid or gas. Depending upon the state of dispersed phase and dispersion medium, eight different types of colloidal dispersions can exist [34]. Types of colloidal dispersions are shown in Table 2.

Particles in the colloidal suspension are greater than 1 μm, they are visible under a microscope and can often be seen with the naked eye [35, 36]. Particles in a suspension will settle on the bottom if the suspension is allowed to stand undisturbed [36].

Table 2. Types of colloidal dispersions [34]

Dispersed Phase	Dispersion Medium	Type of Colloidal Dispersions
Gas	Liquid	Foam
Gas	Solid	Solid foam
Gas	Gas	Does not exist
Liquid	Gas	Liquid Aerosol
Liquid	Liquid	Emulsions
Liquid	Solid	Gel
Solid	Gas	Solid Aerosol
Solid	Liquid	Sol or Colloidal Suspension
Solid	Solid	Solid sol (solid suspension)

Particles in a dispersion medium collide with each other frequently. The stability of colloidal suspensions is therefore determined by the interaction between the particles during such a collision [37]. There are two basic interactions: one being attractive and the other repulsive. When attraction dominates, the particles will adhere with each other and finally the entire dispersion may consolidate. When repulsion dominates, the system will be stable and remain in a dispersed state [37]. Figure 9 shows an example of a stable suspension, as well as an unstable suspension.

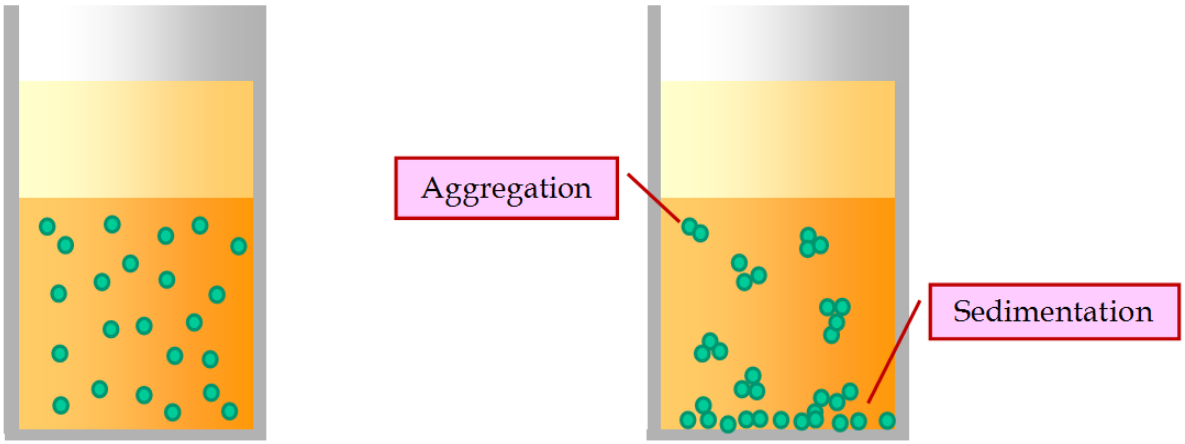

Figure 9. Example of a stable (left) and an unstable suspension (right) [38]

Van der Waals forces are the primary source of attraction between colloidal particles. These forces are always present between particles of similar composition. Therefore, a colloidal suspension is said to be stable only when a sufficiently strong repulsive force counteracts the van der Waals attraction [37].

Since there are always strong attractive forces between similar colloidal particles, it is necessary to provide repulsion between the particles to obtain stability. This repulsion should be at least as strong as the attractive force and comparable in range of the attractive interaction. There are 2 types of stabilization: electrostatic or charge stabilization, and steric stabilization [37]. Combination of these stabilization mechanisms leads to electrosteric stabilization.

In liquid dispersion medium, ionic groups can adsorb to the surface of a colloidal particle through different mechanisms to form a charged layer. To maintain electroneutrality, an equal number of counterions with the opposite charge will surround the colloidal particles and give rise to overall charge-neutral double layers [37]. In charge stabilization, it is the mutual repulsion of these double layers surrounding particles that provides stability. The thickness of the double layer depends on the ionic strength of the dispersion medium [37]. Disadvantage of charge stabilization of particles is its great sensitivity to the ionic strength of the dispersion medium. Additionally, it only works in polar liquids which can dissolve electrolytes [37].

A medium with a low dielectric constant will restrict the dissociation of substances that are normally ionisable in a medium with a high dielectric constant (for instance water) [39]. This property decreases the concentration of the ions in the medium. Many organic solvents have

low dielectric constants, therefore requiring a different stabilization mechanism – steric stabilization [39]. Steric stabilization results from the presence of an adsorbed polymeric layer on the particle surface [40].

The close approach of two coated particles causes compression of their polymer layers. The resulting strong repulsive force provides the steric stability [41]. There are a few requirements for the steric stabilization [42]. The surface of the particle should be completely covered and the polymer layer should be as dense as possible. The polymer should be firmly anchored to the surface so that it cannot be displaced during particle collision. The layer must be thick enough to keep the particles outside of the range of the attractive van der Waals forces. Representations of types of stabilization are shown in Figure 10.

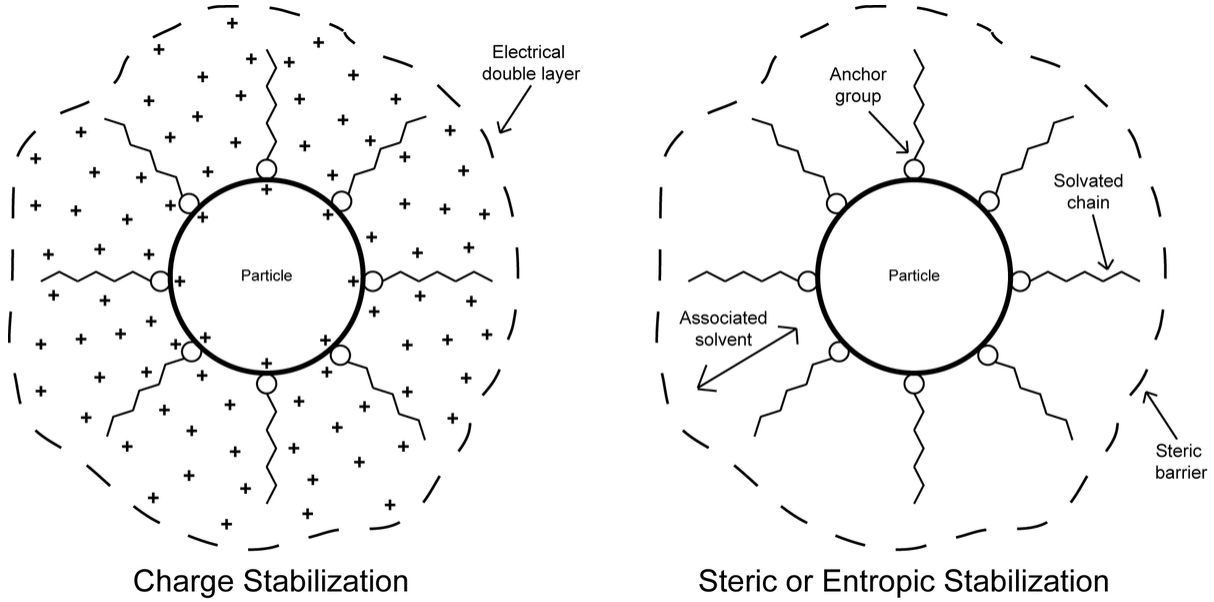

Figure 10. Types of stabilization [31]

1.9. Description of the main thesis task

In the current slurry, which was developed at the Institute, powder particles settle within a few hours. It means the slurry is not stable. Figure 11 shows the current slurry immediately after mixing, as well as 15 days after mixing. It is obvious that the stability of this slurry is not satisfactory, as separation and sedimentation have occurred.

Figure 11. Room temperature stability of the original slurry

When the slurry is unstable, it has to be mixed every time before it is used on the Blueprinter. Improving stability could enable the slurry to be stored for longer periods of time and still be usable immediately when needed. Another downside of poor stability is its effect on the printing. If the settling of the powder particles occurs during printing, the properties of the green part could differ along the vertical axis, therefore resulting in properties which are not as intended. Therefore, improved stability is also beneficial for successful printing with the slurry.

Main goal of this thesis was to improve slurry stability. With the new slurry, appropriate printing parameteres have to be determined. Also, the cleaning of the residual slurry after printing and the thermal treatment have to be determined. In order to have as best as possible

properties of the final part, it is also beneficial to increase the solid loading. The solid loading of the current slurry is 44,9 vol%.

Different stability performance can be obtained by varying the components of the slurry. As stated before, slurries for stereolithography of ceramic materials contain at least one polymerizable liquid organic component, a solvent, a photoinitiator, light absorber, dispersing agent and an inorganic phase in form of ceramic powder.

The main idea for increasing stability is to replace the solvent with a wax. Solvent and wax perform the same role during the thermal treatment, but the difference is that waxes are solid at room temperature. This means that the slurry containing wax could become solid while stored, therefore preventing any settling of the ceramic particles. Varying the monomers, dispersing agents and solvents can also influence rheological properties and stability. By increasing viscosity, there is less movement inside the colloidal suspensions which could result in better stability.

2. MATERIALS AND METHODS

2.1. Materials

2.1.1. Tricalcium Phosphate

The commercially available Tricalcium Phosphate powder was used in this thesis.

2.1.2. Waxes

Five different wax materials were used in this thesis. They are referred to as W1, W2, W3, W4 and W5. They differ in chemical formulas, polarity and molecular chain length. Therefore, they could provide different stability performances.

2.1.3. Solvents

Four different solvents were used in this thesis. They are referred to as S1, S2, S3 and S4. The difference between them is the number of carbon (C) and hydrogen (H) atoms (Figure 12). They also differ in molecular weight, with S1 having the lowest molecular weight and S4 having the highest molecular weight. The higher the molecular weight, the molecules are bigger, therefore increasing the viscosity of the solvent.

Figure 12. Difference between the repeat units of different solvents [43]

2.1.4. Dispersing agents

Eleven different dispersing agents were used in the thesis. They are referred to as D0, D1, D2, D3, D4, D5, D6, D7, D8, D9 and D10. D0, D9 and D10 were tested because they were used in previous studies [21, 39]. Other dispersing agents were chosen for the experiments based on the medium in which the ceramic particles will be dispersed.

2.1.5. Monomers

In this thesis, six different commercially available monomers were used, and they are referred to as M1, M2, M3, M4, M5 and M6. These monomers are of 2 different types (methacrylates and acrylates) and they differ in functionality and viscosity. These properties can also provide different slurry properties, as well as the green part properties.

Of the used monomers, M1 and M3 have the highest viscosity, while M4 has the lowest viscosity. Monomer viscosity can influence the slurry viscosity, therefore resulting in different stability performances.

According to International Union of Pure and Applied Chemistry (IUPAC), the functionality of a monomer is defined as the number of covalent bonds that a monomer molecule can form with other reactants [44]. A difunctional monomer can react with two other monomers and if this process is repeated many times it will lead to the formation of a linear chain. With trifunctional monomers, a branch point can be formed leading to a branched macromolecule [44, 43]. Of the used monomers, M2 is a trifunctional monomer, while others are difunctional.

M1, M3 and M5 are methacrylate monomers, while M2, M4 and M6 are acrylate monomers. Acrylate monomers contain vinyl groups (−CH=CH_2). This implies that there are two carbon atoms double bonded to each other, and directly attached to the carbonyl carbon atom (C=O). When the acrylates have an extra methyl group (CH_3) attached to the alpha carbon, they are called methacrylates [45]. Figure 13 shows polymethyl acrylate and a polymethyl methacrylate. Methacrylate and acrylate monomers differ in their properties, more specifically viscosity before polymerization, hardness when polymerized and polymerization speed.

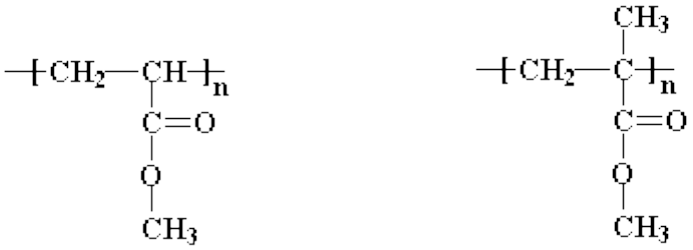

Figure 13. Structure of polymethyl acrylate (left) and polymethyl methacrylate (right) [45]

The hardness of a polymer at a given temperature is determined by chain mobility, which represents how well the polymer chains move and rotate past each other. The higher the chain mobility, the polymer is softer [45]. In polymerized methacrylates, their extra methyl group

inhibits the free movement of the methacrylate chains. Acrylates, on the other hand, can move more freely and are therefore able to flow more easily. Therefore, a polymer with higher chain mobility will be soft, and a polymer with low chain mobility will be hard [45].

Acrylates polymerize much faster than methacrylates [46]. In radical polymerization, an acrylate forms secondary radicals as the propagating end group, while a methacrylate forms tertiary radicals (which are more stable than secondary radicals) (Figure 14). The stability of the tertiary radical is thought to lower the reactivity of the propagating end for further polymerization [47]. Radicals can be considered to be electron deficient, and are therefore stabilized by the electron-donating effects of nearby alkyl groups, for instance methyl group (CH_3) [47].

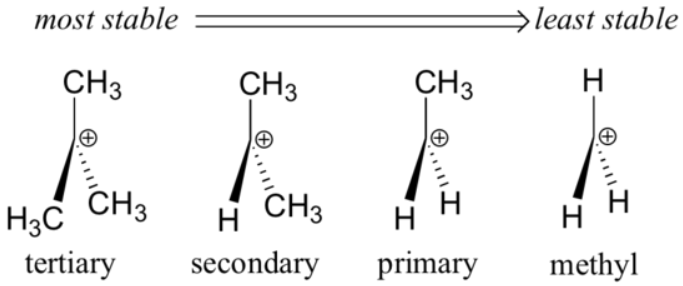

Figure 14. Radical stability [47]

2.1.6. Light absorber

To absorb the scattered light and to prevent overgrowing of the part, a light absorber referred to as LA1 is used. It absorbs the wavelength corresponding to the light used in the Blueprinter. There is no need to test other light absorbers as it doesn't have any effect on slurry stability.

2.1.7. Photoinitiator

As mentioned previously, a photoinitiator is needed to start the polymerization reaction. In this thesis, photoinitiator referred to as PI was used. The light used for its activation matches the light used in the Blueprinter. As with the light absorber, the photoinitiator also doesn't influence the slurry stability. Therefore no other photoinitiators were tested.

2.2. Methods

2.2.1. Preparation of the slurries

A Sartorius lab scale was used to measure the correct amount of each component to be put into the mixture. First, the organic part of the slurry is prepared. The components are put in a plastic mixing cup starting from the most viscous component. If a wax is used, the mixture is placed in the furnace at the appropriate temperature to allow the melting of the wax. Next, the ceramic powder is introduced gradually in order to obtain easier mixing. Afterwards, a mixing device (Speedmixer), which is based on the double rotation of the mixing cup, is used to achieve a homogeneous mixture. The parameters used were 30 seconds at 3500 rpm. In each experiment, only one component or parameter at a time was varied in order to observe its effect on slurry stability and printing quality.

2.2.2. Stability tests

All of the newly prepared slurries were submitted to two stability tests. Each slurry was separated into two glass tubes. One of them was stored at room temperature for 15 days, while the other was placed into the furnace at 70°C for 72 hours. The stability at an elevated temperature was tested because most of the slurries contained waxes, which have a higher melting point compared to other components. As the Blueprinter requires the slurry to be liquid, it is necessary to heat up the slurry containing wax before printing. It is also necessary to keep the vat of the Blueprinter at a specified temperature, in order to maintain the liquid state of the slurry. A stability test of 72 hours was chosen to ensure the stability could be maintained during the whole printing process. Longer test was not needed as no printing process will take longer than the stated 72 hours. During the tests, notes and pictures were taken in order to track the changes that occurred, and to observe the stability performance of each slurry. The slurries were then compared by their room temperature and elevated temperature stability.

2.2.3. Printing tests

Printing quality was tested by using the Blueprinter to print test structures with the selected slurries. Three test structures were used: a cylinder, a plate with holes (German: *Loch Platte*) and a cylinder bone structure. They are shown in Figure 15.

Figure 15. Structures used for testing of the printing quality

30 layers of test structures using layer thickness of 25 μm were printed. The shape and the appearance of the test structures were then compared to the expected and designed shape. For instance, the cylinder bone structure was compared to the STL file sliced at the 30th layer (Figure 16). Afterwards, the slurries were compared by the printing quality they provided.

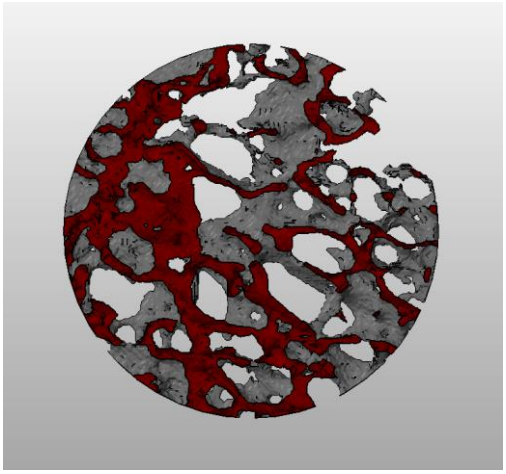

Figure 16. 30th layer of the bone structure

Before the printing, it was necessary to determine the appropriate parameters for printing of the each slurry. That was done by exposing the slurry to the light only once, and then measuring the curing depth. In a previous study [29], a curing depth of 100 μm for layer thickness of 25 μm was used. In this case, the layer thickness is also set to 25 μm. The curing depth of approximately 150 μm was chosen to be the goal, to ensure a successful printing job and the subsequent thermal treatment. The parameters that influence the curing depth are exposure time and light intensity. These parameters were varied in order to achieve the required curing depth. Once determined, they were used for the corresponding slurry. With

the heating system, the vat was kept at an elevated temperature for the wax slurries during the printing process. The temperature used was 70 °C.

It is beneficial to keep the exposure time as short as possible in order to achieve a printing process which is not time consuming. At the same time, it is necessary to keep the printing quality at the desired level, which requires a fine balance between the exposure time and the light intensity used.

2.2.4. Rheology measurements

The selected slurries were subjected to a rheology test in order to measure the viscosity. As mentioned previously, the maximum allowed viscosity of the slurry to be used on the Blueprinter is 20 Pa s [22]. In this test, Anton Paar Physica MCR 301 rheometer was used. It is a rotational rheometer that works with a cone and horizontal plate, and it controls the applied shear stress [39]. A cone with a diameter of 25 mm and the angle between the cone surface and the plate of 1° was used. The horizontal plate temperature was set to 50°C in order to keep the slurries in a liquid state.

2.2.5. Wax variation

In this experiment, the waxes were tested. The composition was based on the slurry used in [21] and [23], which is shown in Table 3. Instead of a solvent, the waxes were used, resulting in 5 new slurries.

Table 3. Slurry composition used in a previous study [23]

Component	[wt%]
Triacrylate monomer	8,77
Dimethacrylate monomer	7,81
Solvent	10,50
Dispersing agent	0,877
Light absorber	0,003
Photoinitiator	0,04
TCP	72,00

2.2.6. Solvent variation

In order to observe the effect of different solvents on slurry stability, three of the previously mentioned solvents were tested: S1, S3 and S4. This experiment resulted in three new slurries, and the composition was also based on the slurry shown in Table 3.

2.2.7. Wax-solvent combination

Different wax-solvent combinations were also tested. The slurry composition for this experiment was based on the slurry shown in Table 3. The total amount of wax was kept the same, except now it was divided between wax and solvent in different ratios. The ratios used were: 20 wt%-80 wt%, 50 wt%-50 wt% and 80 wt%-20 wt%. The wax used in all variations was W1, while three differents solvents were used for each ratio (S2, S3 and S4). This experiment generated 9 new slurries.

2.2.8. Wax-monomer compatibility

Prior to monomer variation, a test was carried out to examine the compatibility between waxes and monomers. Waxes W1, W3 and W4 were used as well as monomers M2, M3 and M4. The mixtures were put into the mixing cups and stored for 5 days. Afterwards they were examined to observe the changes that occured.

The combinations were as follows:

- W3, M3, M2
- W1, M3, M2
- W4, M3, M2
- W4, M2
- W4, M4.

2.2.9. Monomer variation

Different monomer combinations have been tested. Tested monomers were M1, M2, M3, M4 and M5. There were 4 combinations:

- M1, M2, M4,
- M1, M2,
- M1, M4,
- M3, M5.

For the first three combinations, different ratios between monomers have been tested, while keeping the same total amount of monomers as in Table 3. For the last combination, only one ratio of monomers was tested.

By using a highly viscous monomer M1, and combining it with lower viscous monomers, it was attempted to improve slurry stability. The combination of M3 and M5 was previously used in [21], and it was tested in this thesis to observe its effect on slurry stability.

2.2.10. Addition of wax

Based on their stability performance, selected compositions of the slurries from the monomer variation experiment have been used for this experiment. Here, the total amount of solvent was divided between wax and solvent in the following ratios (wax-solvent): 20 wt% - 80 wt% and 30 wt% - 70 wt%. The intention of this experiment was to try and improve the stability of the slurry with the addition of wax. The waxes used were W1 and W4.

2.2.11. Increase in monomer content

Increasing the monomer content in the slurry could provide better printing quality, as more reactive components are present. Therefore, slurry compositions that showed promising results on the previous stability and printing tests were selected for this experiment. Also, a slurry with even higher wax content was tested to determine if it can achieve the required printing quality while improving the stability. Therefore, the tested ratios of wax and solvent in this experiment were 30 wt% - 70 wt% and 40 wt% - 60 wt%. The monomer increase is achieved at the expense of total wax and solvent content. In the new slurries, monomer content was increased by 5 wt% and 10 wt%.

2.2.12. Photoinitiator and light absorber content

In order to improve the printing quality, it is important to optimize the light absorber content and the photoinitiator content. Four new slurries were prepared, each containing different amount of light absorber, ranging from 0,007 wt% – 0,018 wt% of the total slurry.

It is also important to optimize the photoinitiator content. Therefore, 2 new slurries have been prepared, with the photinitiator content ranging from 0,044 wt% – 0,066 wt% of the total slurry.

As the light absorber and photoinitiator content don't influence the slurry stability, these slurries have only been tested concerning printing quality. After comparing the results, the appropriate content of each component has been determined.

2.2.13. Dispersing agents

In order to further optimize the slurry, after testing all the other components, the previously mentioned dispersing agents have been tested. Stability and printing quality tests have been carried out with the new slurries. After comparing the results, a few of the slurries have been immediately eliminated from further testing because of their poor performance.

2.2.14. Increase in solid loading

As it would be beneficial to have solid loading as high as possible, the performance with increased solid loading was tested. Six of the remaining dispersing agents have been used to prepare slurries with solid loading ranging from 49,7 vol% – 52,3 vol%.

After analyzing the results of this experiment, the best performing dispersing agent was chosen, as well as the appropriate solid loading.

2.2.15. Cleaning procedure

After printing, there is still some residual slurry on the green part. Therefore, before the green part is subjected to the thermal treatment, it needs to be cleaned. An appropriate cleaning procedure needs to be determined, which cleans the green part completely, and at the same isn’t too aggressive to cause damage to the printed structure.

The cylinder bone structure has been used to test different cleaning procedures. Three cleaning procedures have been tested, each procedure with 5 or 6 different cleaning solvents. Solvents used were named: CS1, CS2, CS3, CS4, CS5 and CS6.

Manual cleaning was as follows. Solvents were heated to 50°C, as well as the water in the ultrasonic bath. Cylinder bone structure was also heated. Solvent was then poured over the bone structure, and put into the ultrasonic bath for 3 minutes (Figure 17). Afterwards, a pipette was used to pressure the solvent onto the bone structure.

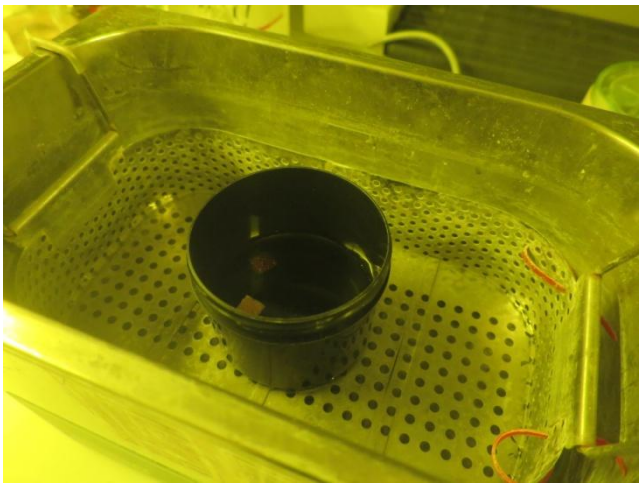

Figure 17. Cleaning of the bone structure with the ultrasonic bath

Two types of machine cleaning procedures were used. In both of them, the solvent and the bone structure were heated. One procedure used solvent flowing from the top (Figure 18, Figure 19). The other was set up in such a manner that the solvent flows over the part from the top and the bottom, and additionally, the ultrasonic bath was used (Figure 20). Both procedures were used for 5 minutes and with the flow rate of 1,4 l/min. The efficiency of these 3 procedures was then compared by examining the cleaned parts using the Carl Zeiss AxioLab light microscope and a scanning electron microscope (SEM).

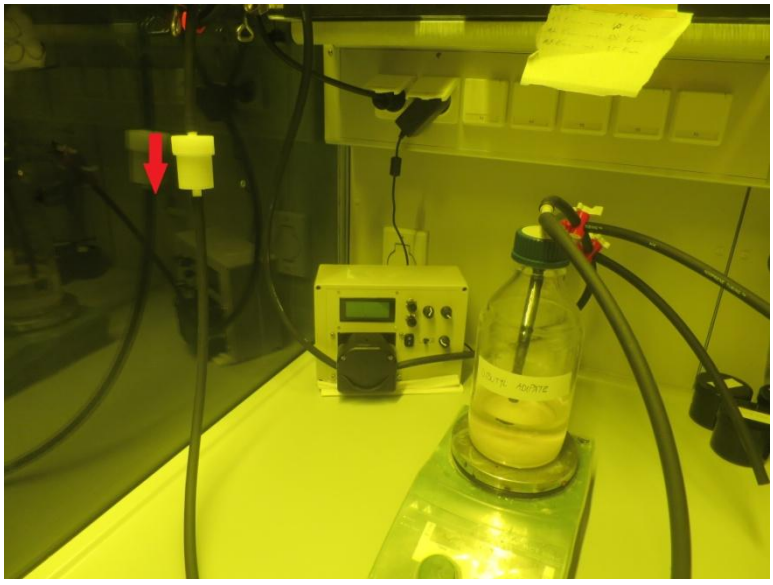

Figure 18. Machine cleaning with solvent flowing from the top

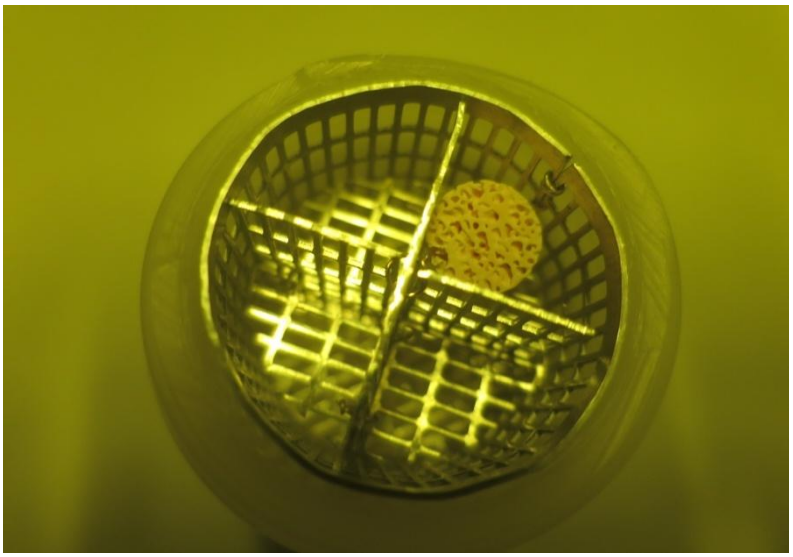

Figure 19. Bone structure inside the cleaning chamber

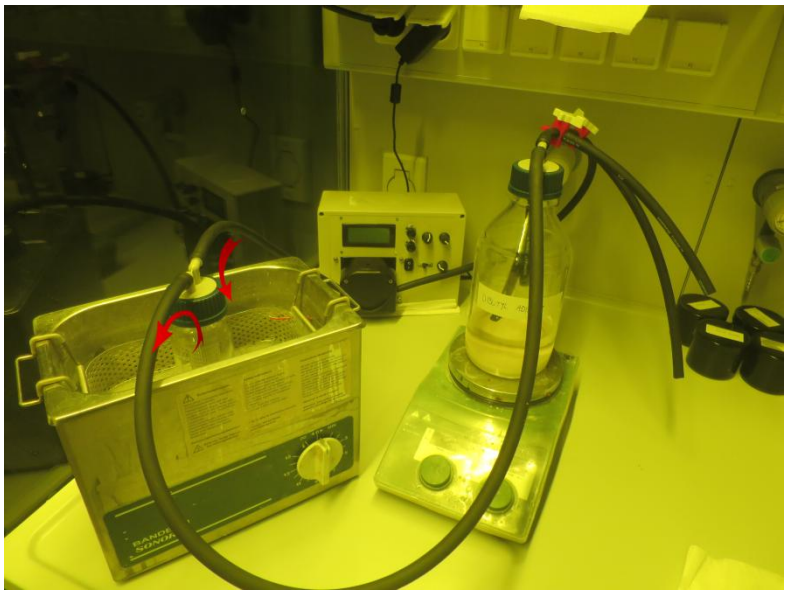

Figure 20. Machine cleaning with solvent flowing from top and bottom

During handling of the cleaned parts, it was noticed that they have absorbed a portion of the solvent. This could influence the size of the green part, therefore the magnitude of the swelling needs to be identified. An experiment has been conducted to determine to what degree each solvent causes the swelling. Graduated bars were printed, and then manually cleaned with the solvents (Figure 21). The dimensions of each bar were measured and the bar was then placed in the respective solvent for 24 hours. After 24 hours, they were measured

once again in order to observe the possible difference in size. This experiment demonstrated which solvent causes the least swelling of the green part.

Based on the results from these experiments, the appropriate cleaning procedure and the appropriate solvent were determined.

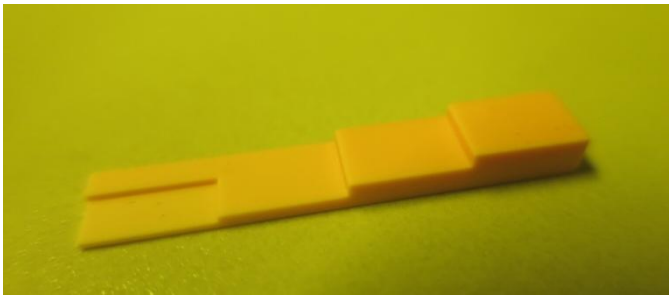

Figure 21. Graduated bar for the swelling experiment

2.2.16. Thermal analysis

Debinding rates need to be carefully adjusted to the volume of the green part in order to avoid cracks in the final structure [29]. Therefore, as mentioned previously, it is necessary to conduct a thermal analysis of the green part.

Thermogravimetric Analysis (TGA) measures the amount of weight change of a material, either as a function of increasing temperature, or isothermally as a function of time, in an atmosphere of nitrogen, helium, air, other gas, or in vacuum [48]. Thermomechanical Analysis (TMA) determines dimensional changes of solids, liquids or pasty materials as a function of temperature and/or time under a defined mechanical force [49]. Using TMA, cracks during debinding of the green part can be seen as a peak in the rate of shrinkage [29].

Cylinders with 6 mm diameter and 5 mm height were used for the TGA, while cylinders with 8 mm diameter and 10 mm height were used for the TMA.

In the first step of the TGA, the green part was heated up from 30 °C to 500 °C with a heating rate of 1K/min for measuring the weight loss in dependence on temperature (Figure 22). Depending on the results, the parameters were gradually adjusted in order to achieve an approximately constant weight loss rate. In the first step of the TMA, the programme obtained from the TGA was used. The parameters were again adjusted in each step to obtain an optimized heating programme.

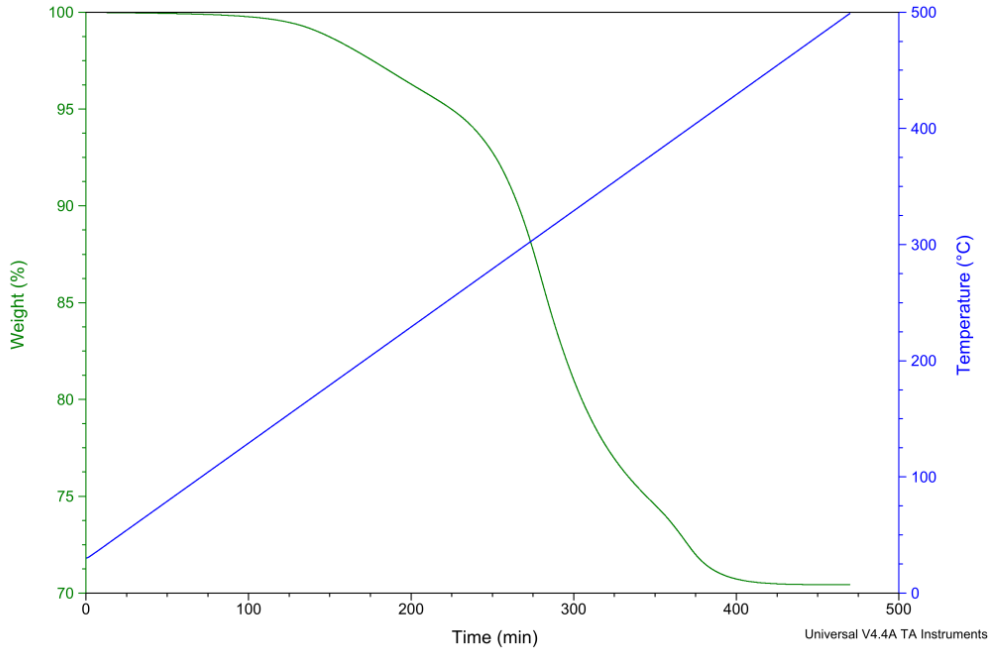

Figure 22. Initial TGA measurement

3. RESULTS AND DISCUSSION

3.1. Stability and printing quality

The wax variation experiment resulted in excellent room temperature stability for 4 out of 5 slurries. The results can be seen in Figure 23. All of the slurries turned solid after only 1 day.

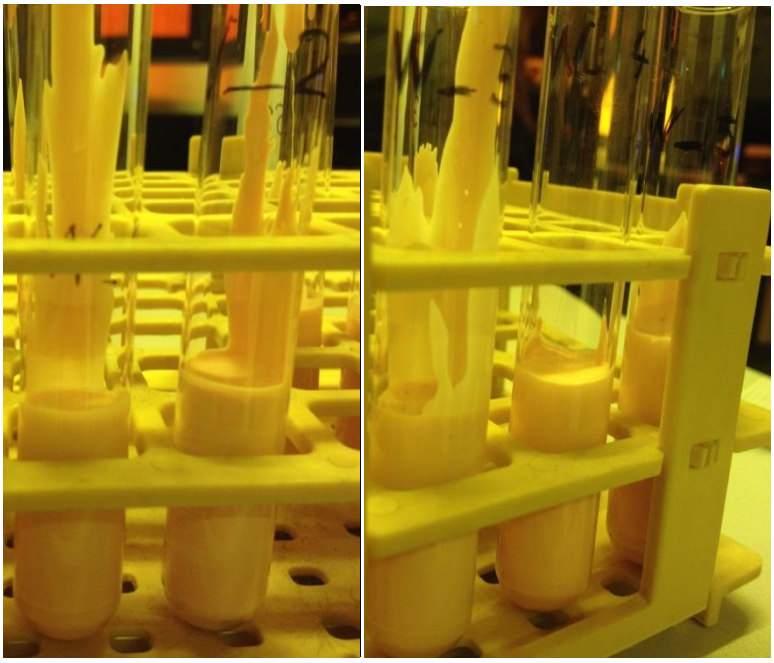

Figure 23. Room temperature stability of wax variation slurries

The only one that didn't have satisfactory stability is the slurry named W_5, which contained wax W5. This slurry showed signs of separation in the form of holes on the surface, which could indicate that the compatibility between the components is not adequate (Figure 24).

Figure 24. Separation of components in the slurry

Concerning stability at 70 °C, Figure 25 shows that slurry W_2 containing wax W2 has better stability than the rest. The stability at 70 °C is, as expected, not at the same level as stability at room temperature. It is, however, much better compared to the currently used slurry (Figure 26).

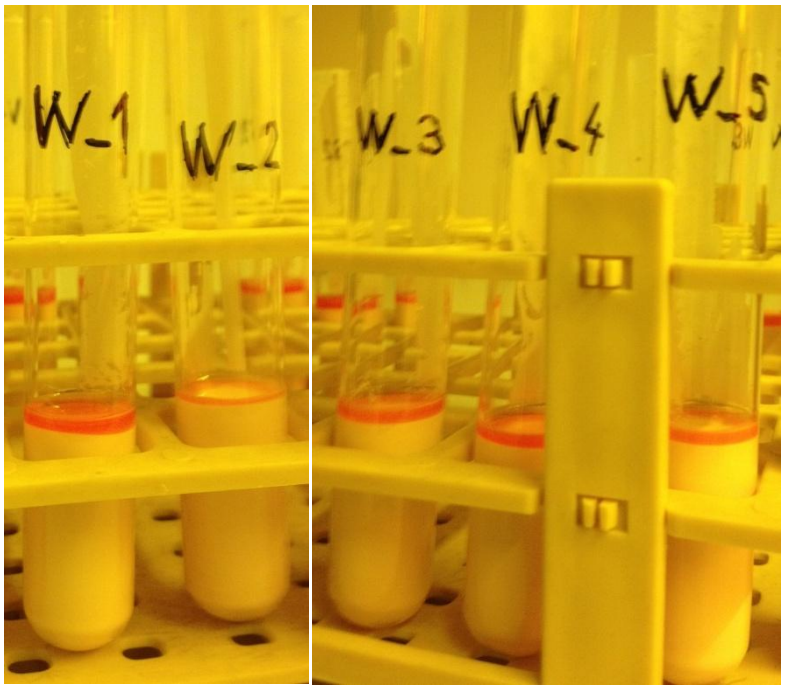

Figure 25. Stability at 70 °C of wax variation slurries

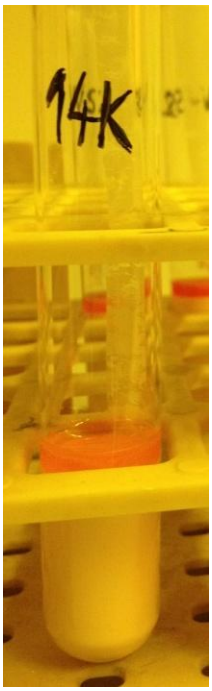

Figure 26. Stability at 70 °C of the currently used slurry

The results of solvent variation are shown in Figure 27. It is obvious that slurries with higher molecular weight solvents offer better overall stability, but they also have higher viscosity.

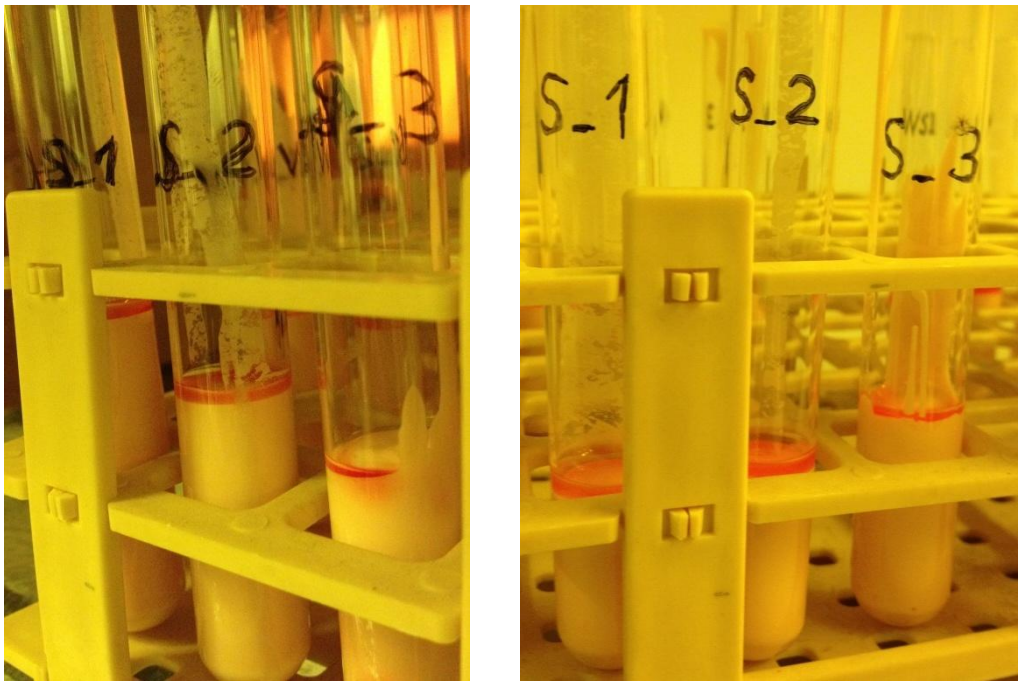

Figure 27. Stability at room temperature (left) and at 70 °C (right) of solvent variation slurries; molecular weight of the solvents increases from left to right

By combining wax and solvents, it was noticed that the slurries with higher wax content have better overall stability (Figure 28 and Figure 29). Slurries with wax-solvent ratio of 80 wt%-20 wt% have shown to have much better stability compared to the other samples in this experiment. This experiment also confirmed the previous result that by using the higher molecular weight solvents the slurry stability is improved.

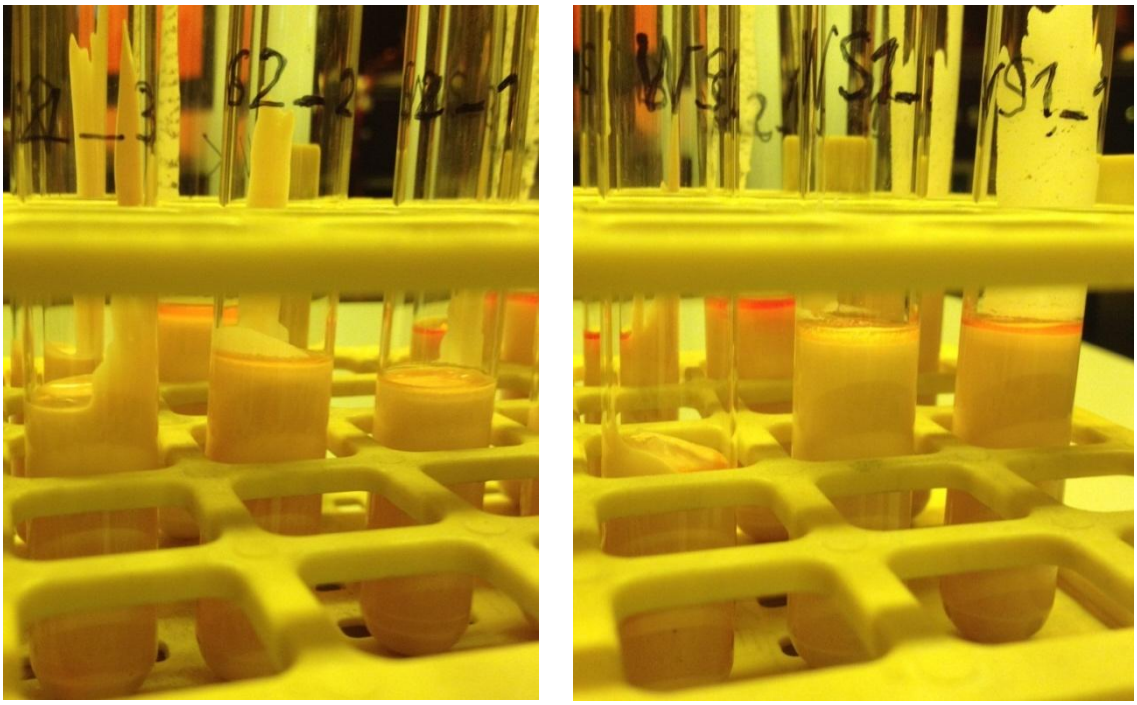

Figure 28. Stability at room temperature for wax-solvent ratio of 50%-50% (left) and 20%-80% (right); molecular weight of the solvents increases from right to left

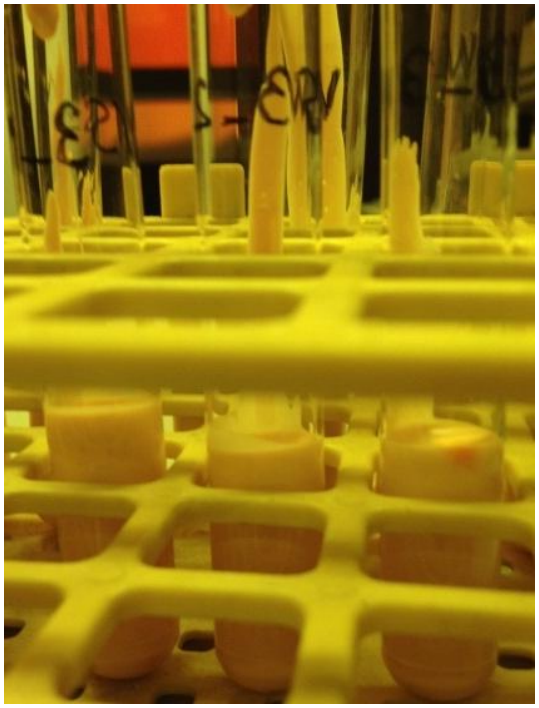

Figure 29. Stability at room temperature for wax-solvent ratio of 80%-20%; molecular weight of the solvents increases from right to left

In the wax-monomer compatibility experiment, it was noticed that the mixture containing monomers M2 and M3 mixed with waxes W1 and W3, respectively, does not have the adequate compatibility. These mixtures had drops of liquid on the surface, which can be described as "sweating" (Figure 30). It shows that the components didn't mix well enough, which can then influence stability if these components are used in the slurry.

Figure 30. Compatibility test for M2 and M3 with: W3 (left), W1 (center), W4 (right)

Also, W4 mixed with monomer M4 doesn't have the adequate compatibility, as the mixture is not homogeneous. On the other hand, W4 combined with M3 and M2, as well as with M2 alone, provided good compatibility, which is demonstrated by the resulting homogeneous mixture (Figure 30 – right, Figure 31 – left).

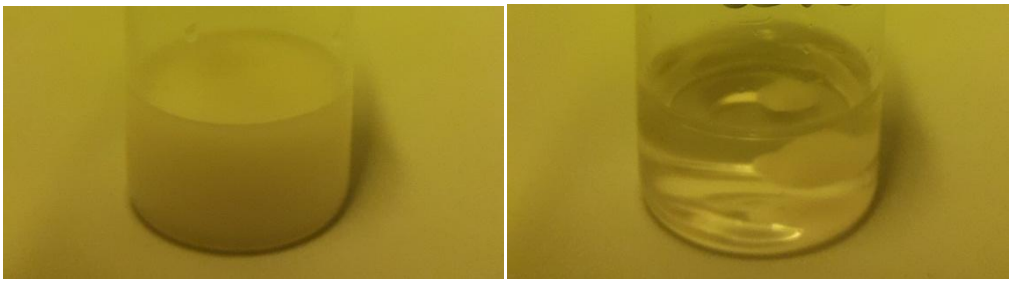

Figure 31. Compatibility test for W4 with: M2 (left), M4 (right)

The reason for these results could be in the polarity of the components. Monomers are mostly nonpolar. W1 and W3 have the chain with C-atoms only on one side of oxyethylene groups (OCH_2CH_2), while on the other side there is the hydroxyl group (OH), which is polar. Therefore, W1 and W3 are more polar than monomers, and it influences their compatibility. W4 is more nonpolar because it has a chain with C-atoms on both sides of the oxyethylene groups. That is the reason why W4 is more compatible with monomers compared to W3 and

W1. It is favourable to have good compatibility between components, otherwise compatibility issues could cause poor stability performance.

Slurries which contained higher amount of monomer M1 demonstrated improved stability (Figure 32). It was expected, as it is a highly viscous monomer. In the slurries which contained three monomers (M1, M2 and M4), with lower content of the monomer M1, the stability was not satisfactory (Figure 33). It could be explained by poor compatibility between the monomers, specifically M2 and M4. Although they are both acrylates, the reason for their incompatibility could be the different shape of the molecules. M4 has more linear molecules, while M2 has branched molecules. M3 and M5 also didn't provide an adequate stability.

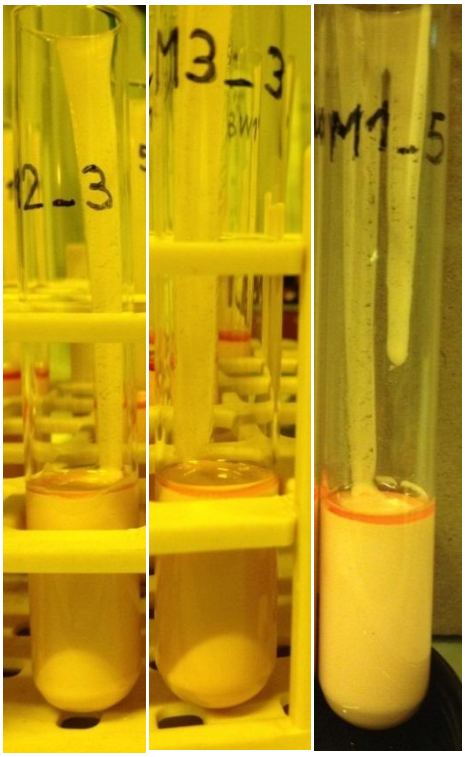

Figure 32. Stability at room temperature for slurries with higher content of M1

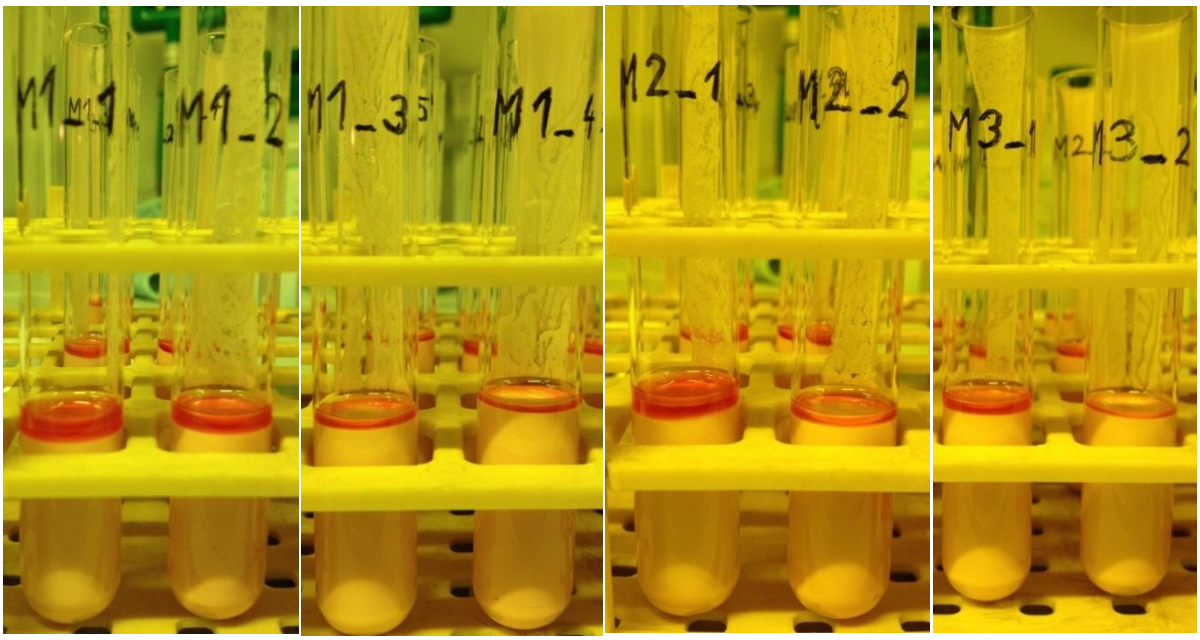

Figure 33. Stability at room temperature for slurries with lower content of M1

Slurries containing M1, with the addition of wax, showed no improvement concerning stability in comparison to the slurries with same monomer combination. In some cases the stability has even worsened (Figure 34). When comparing Figure 34 and Figure 35, it can be concluded that W4 provides better stability than W1.

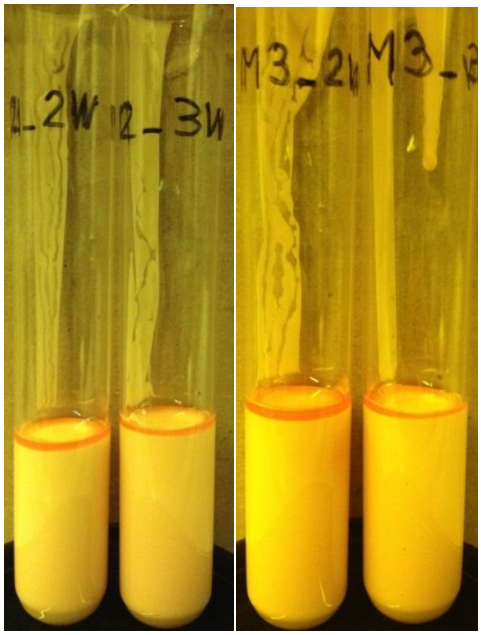

Figure 34. Stability at room temperature for monomer variation slurries with the addition of W1 (wax-solvent ratio: 20 wt%-80 wt%)

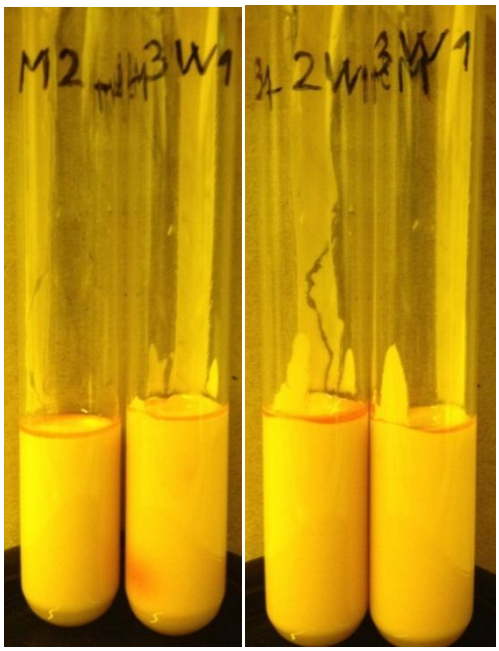

Figure 35. Stability at room temperature for monomer variation slurries with the addition of W4 (wax-solvent ratio: 20 wt%-80 wt%)

Here, another monomer was tested with M3, it was M6. This combination didn't provide good stability (Figure 36 – right). In case of M5 and M3 combination, the addition of wax provided improvement regarding stability of the slurry (Figure 36 – left). The slurry with wax-solvent ratio of 30 wt%-70 wt% was no longer liquid after 3 days, which could be a great advantage concerning stability.

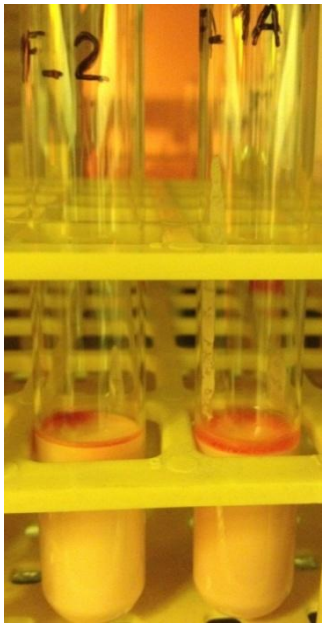

Figure 36. Room temperature stability for the combination of M3 with M5, wax-solvent ratio: 30 wt%-70 wt% (left); and M3 with M6, wax solvent ratio: 20 wt%-80 wt% (right)

The only difference between M6 and M5 is that the former is an acrylate and the latter is a methacrylate. This experiment proved that the compatibility, and therefore the stability, is better when using methacrylate monomer in combination with another methacrylate. In this case, it is better to use M3 in combination with M5, instead of M6.

At this point, printing tests were carried out with the selected slurries. Slurries from the wax variation and wax-solvent combination experiments could not be used for printing, as the printed parts were not strong enough. With most of them, the test structure *Loch Platte* broke down at the 20th layer, where there is a big difference in cross section. Slurries containing monomer M1 also proved to have inadequate strength for the printing. Combination of M3 with M5 demonstrated good printing quality (Figure 37).

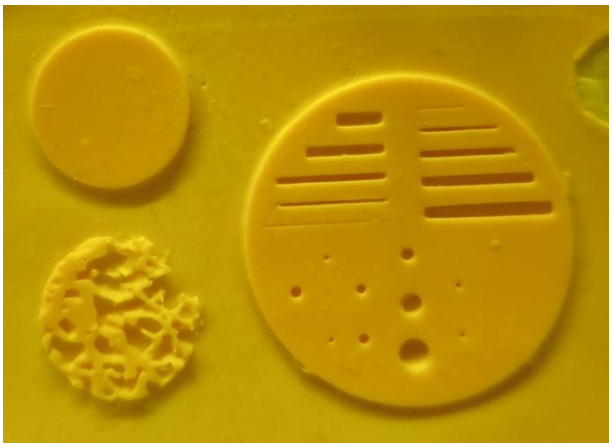

Figure 37. Printing quality of the slurry containing M3 and M5

Addition of wax to the slurry with M3 and M5 influenced the printing quality negatively, as some details were missing from the printed parts (Figure 38).

Figure 38. Printing quality of the slurry containing M3 and M5, with wax-solvent ratio of 20 wt% - 80 wt%

Based on the printing quality results, and the stability results up to this point, the selected wax was W4, while selected monomers were M3 and M5. Also, solvent S2, with low molecular weight, was chosen for further use.

As the printing quality still needed to be improved, monomer content was increased. The results of the increase in monomer content regarding stability and printing quality are shown in Figure 39 and Figure 40. It can be seen, when comparing Figure 39 to Figure 38 that increasing the monomer content improves the printing quality, while comparing Figure 40 to Figure 36, that the stability is still adequate. For the slurry with wax-solvent ratio of 40 wt%-60 wt%, the printing quality was not satisfactory (Figure 41). It was also determined that a 10 wt% increase in monomer content is too high, as it worsened the stability (Figure 40 – right). The slurry with a 5 wt% increase in monomer content and wax-solvent ratio of 30 wt%-70 wt showed good printing quality, while maintaining the adequate stability.

Figure 39. Printing quality of the slurry with 5 wt% increase in monomer content and wax-solvent ratio of 30 wt%-70 wt%

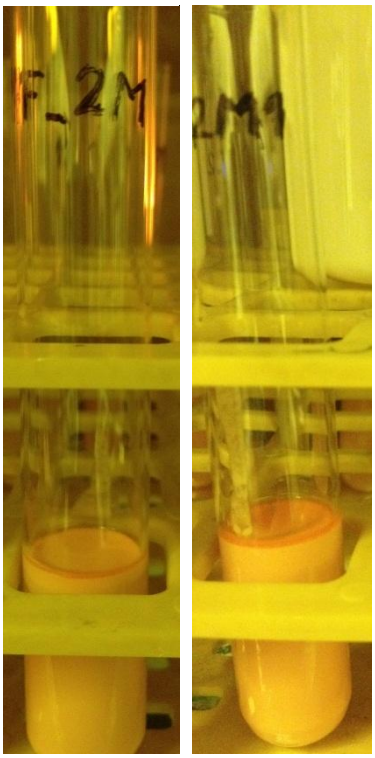

Figure 40. Room temperature stability of the slurry with wax-solvent ratio 30 wt%-70 wt%: 5 wt% increase in monomer content (left), 10 wt% increase in monomer content (right)

Figure 41. Printing quality of the slurry with 5 wt% increase in monomer content and wax-solvent ratio of 40 wt%-60 wt%

The printed parts for the optimization of the light absorber content are shown in Figure 42 and Figure 43. These results show that increasing the absorber content provides better printing quality. However, using more absorber means that the required light intensity is higher. Also the required exposure time is longer. For the slurry with the lowest amount of absorber a light

intensity of 45 mW/cm^2 and exposure time of 16 s (base layers) and 12 s (other layers) were used, while for the highest amount a light intensity of 58 mW/cm^2 and exposure time of 22 s were used. If higher light intensity is used, there is a higher amount of scattered light, and therefore more overgrowing of the part occurs. In that sense, it is favourable to use the lower light intensity while keeping the required printing quality.

Figure 42. Printing quality with absorber content of 0,007 wt% (left) and 0,012 wt% (right)

Figure 43. Printing quality with absorber content of 0,018 wt%

By comparing these printed parts, it was determined that absorber content of 0,018 wt% was too high, as the printing quality was not evidently better compared to the second highest absorber content (0,012 wt%). As the printing quality with lower contents was not satisfactory, the absorber content of 0,012 wt% was selected as the optimum. The light intensity used for this slurry was 58 mW/cm^2, while the exposure time of 22 s (base layers) and 18 s (other layers) was used.

In order to decrease the exposure time, higher light intensity was used to achieve the required curing depth. With that, it was possible to decrease the exposure time to 10 s, and the light intensity was then increased to 89 mW/cm^2. The printing quality did not decrease with these new parameters.

The printed parts for the optimization of the photoinitiator content are shown in Figure 44. The printing quality was very similar with all of the tested slurries. As the increase in photoinitiator content allowed the decrease of the light intensity from 89 mW/cm^2 to 63 mW/cm^2, the highest photoinitiator content (0,066 wt%) was determined as the optimum.

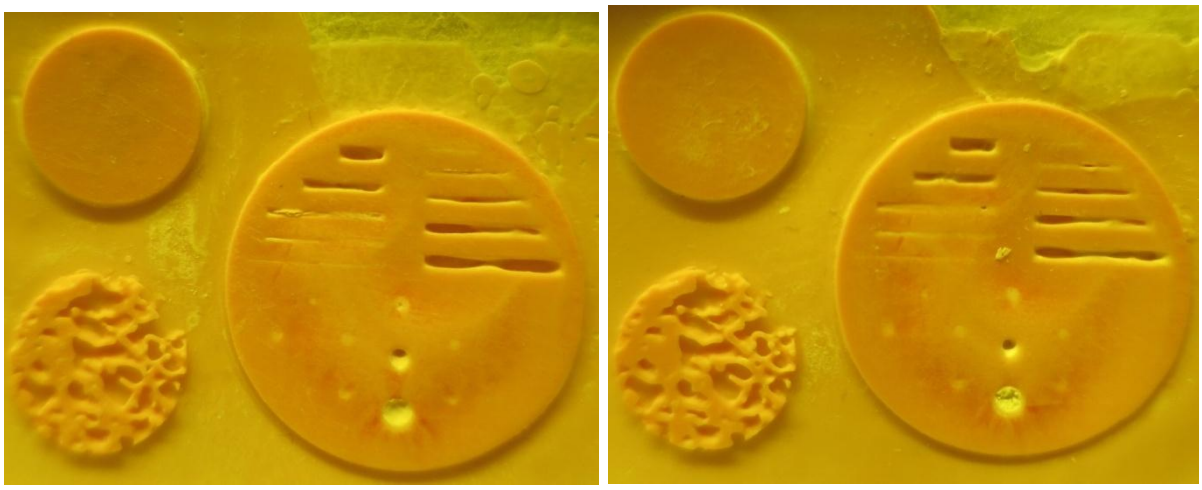

Figure 44. Printing quality with photoinitiator content of 0,044 wt% (left) and 0,066 wt% (right)

Slurries containing D1, D2, D9 and D10 as dispersing agent were eliminated shortly after preparation because of the resulting slurry viscosity (Figure 45). The viscosity was too high and they could not be used on the Blueprinter. The slurry containing D7 was also eliminated. Results of other slurries are shown in Figure 46.

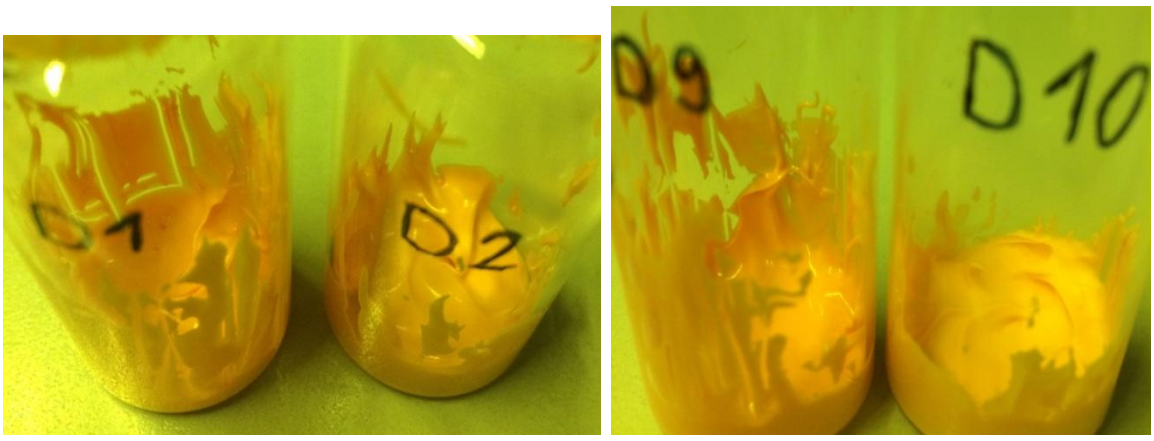

Figure 45. Slurries containing D1, D2, D9 and D10

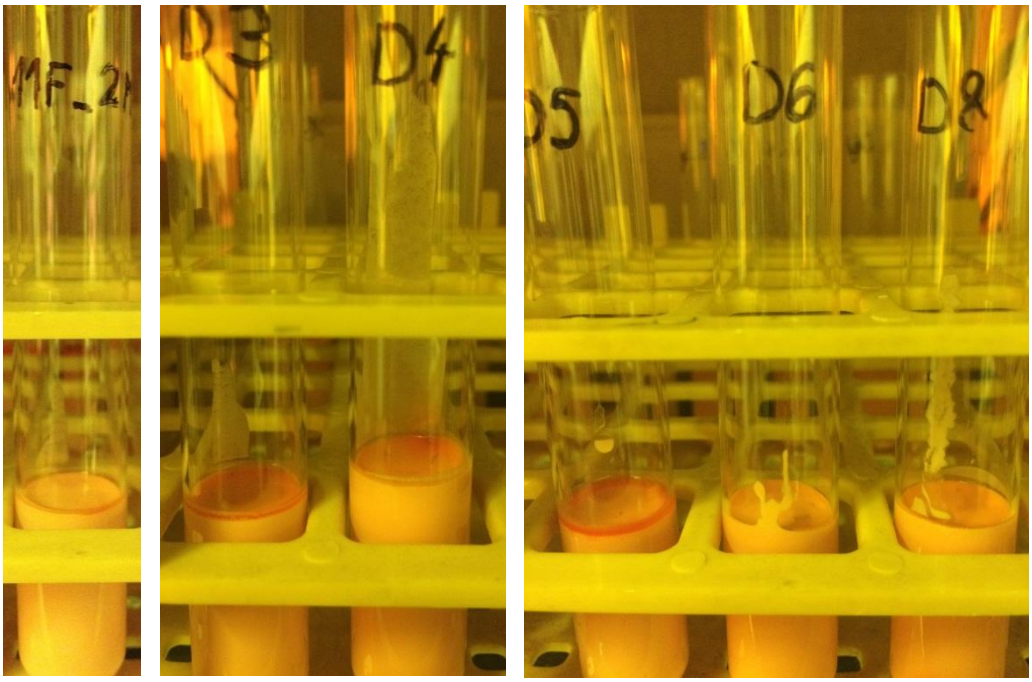

Figure 46. Room temperature stability of slurries with different dispersing agents

After using the remaining dispersing agents for preparation of the slurries with increased solid loading, they were tested for their stability and printing quality. The results of the stability tests are shown in Figure 47. When comparing Figure 46 with Figure 47, it can be observed that the increased content of TCP resulted in better stability.

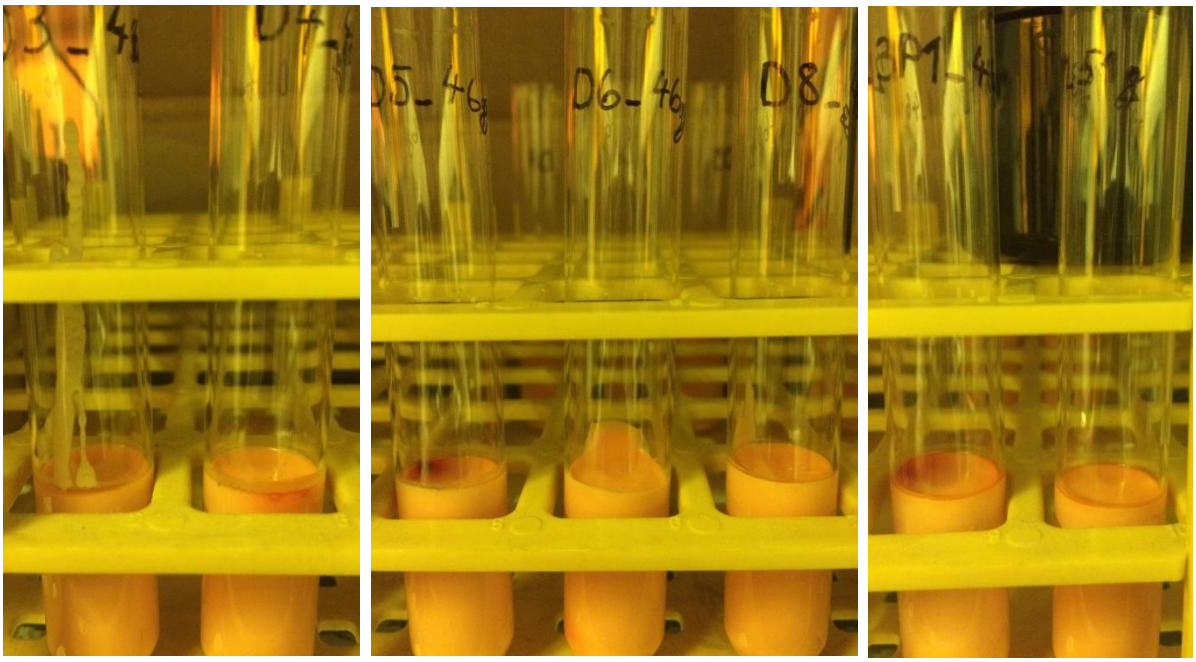

Figure 47. Room temperature stability of slurries with different dispersing agents and increased solid loading

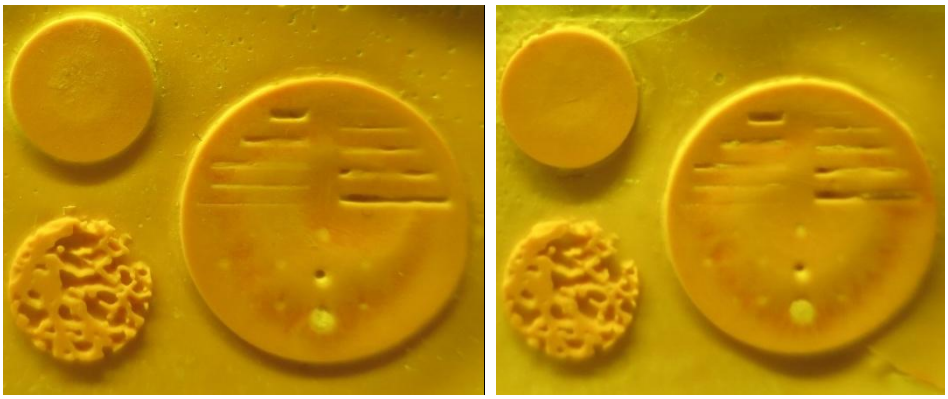

Figure 48. Printing quality of the slurry with 49,7 vol% (left) and 52,3 vol% (right)

When using solid loading of 52,3 vol%, the printing quality decreases, while with 49,7 vol% the printing quality was still the same as with lower solid loading (Figure 48). Therefore it was determined that the solid loading of 49,7 vol% was the optimum, as it provides better stability while keeping the printing quality at the desired level. Three of these slurries demonstrated best stability, and the easier processing during printing determined that the slurry containing D4 had the best overall properties (Figure 49).

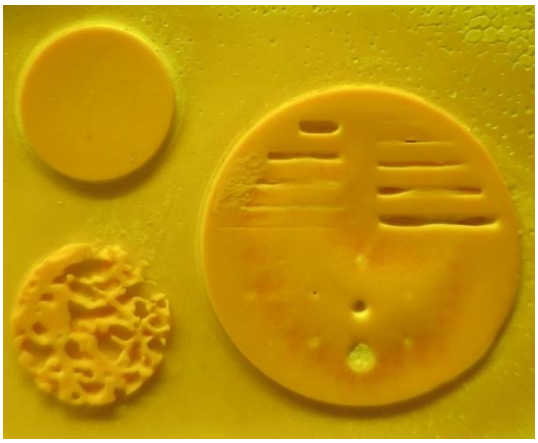

Figure 49. Printing quality of the slurry with D4 (light intensity: 63 mW/cm^2)

With these experiments, a stable slurry with increased printing quality was achieved. After further tests on the Blueprinter, the light intensity was decreased from 63 mW/cm^2 to 36 mW/cm^2 without compromising the printing quality (Figure 50). It was determined that a curing depth of approximately 100 μm is sufficient to achieve the desired printing quality. The composition of this slurry is shown in Appendix, and the printing parameters are shown in Table 4.

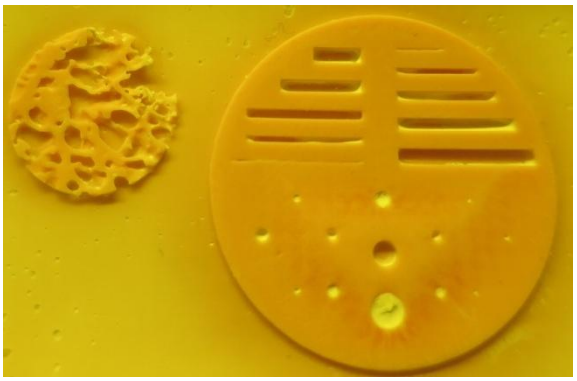

Figure 50. Printing quality of the slurry with D4 (light intensity: 36 mW/cm^2)

Table 4. Printing parameters for the final slurry (FK_11F_2M_3P1_D4_46g)

Light intensity:	36 mW/cm^2
Exposure time:	12 s
Layer thickness:	25 μm
Resolution X-Y:	25 μm

3.2. Rheology measurements

The results of the rheology measurements, which are shown in Figure 51, demonstrate that all of the tested slurries have the appropriate viscosity. The reason why some slurries have fluctuating values can be due to the fact they have been previously used on the Blueprinter. It means that cured particles can be found in the slurry, and they can influence the rheology measurements, causing the appearance of the peaks. From these results, it can be seen that the viscosity increases with higher solid loading (FK_11F_2M_3P1_D4_46g has higher viscosity compared to FK_11F_2M_3P1_D4 in the graph). The results also show that the addition of wax does not increase viscosity (FK_11F_3M_3 does not have higher viscosity compared to FK_11F_2M_3P1), while the use of different dispersing agents can influence rheological behaviour of the slurry (FK_11F_2M_3P1 compared to FK_11F_2M_3P1_D4).

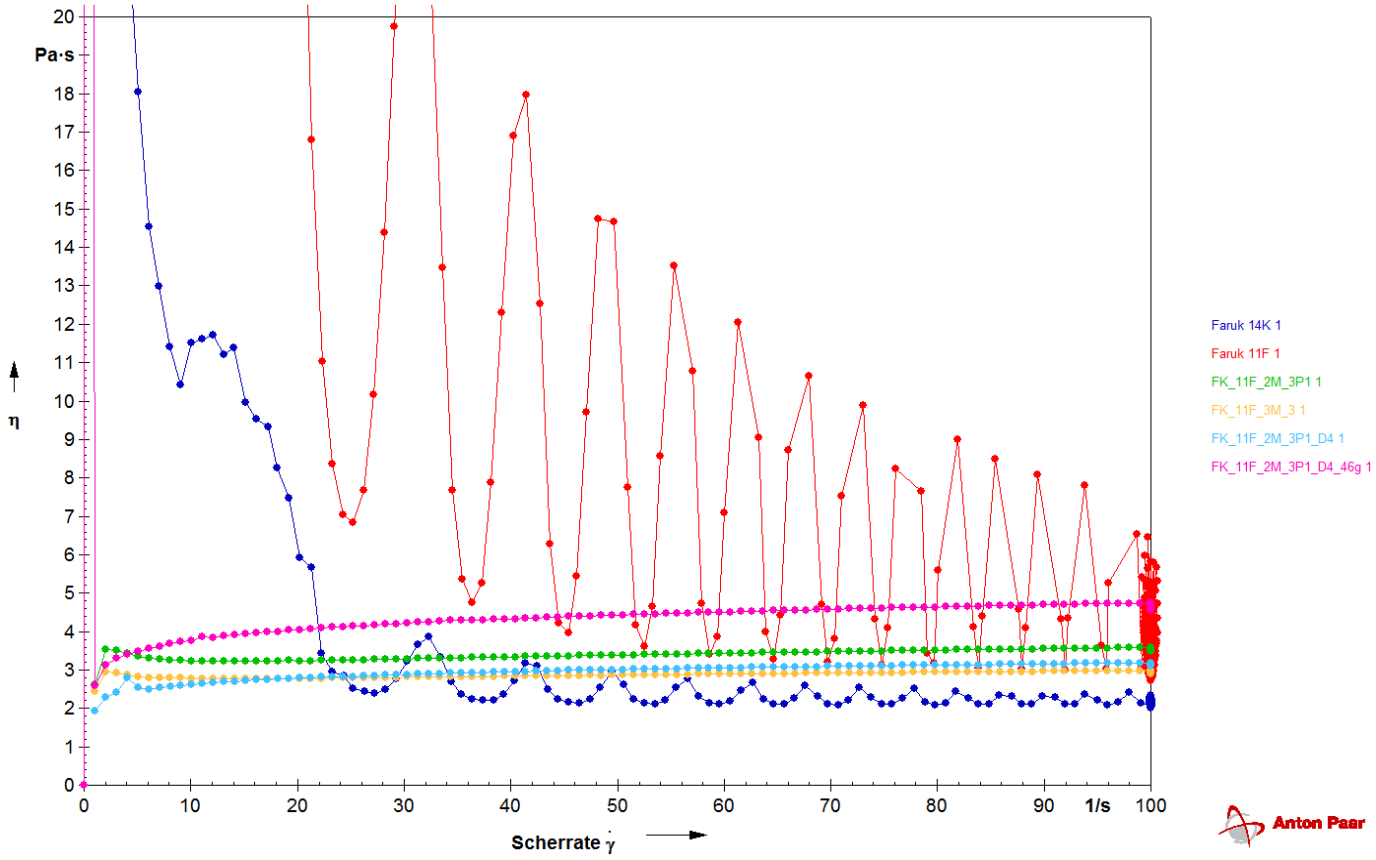

Figure 51. Viscosity measurements

3.3. Cleaning procedure

Cross sections of the manually cleaned parts are shown in Figure 52, Figure 53 and Figure 54. These results show that, except CS3, all the other solvents can clean the part efficiently. Therefore, CS3 was not used for the machine cleaning.

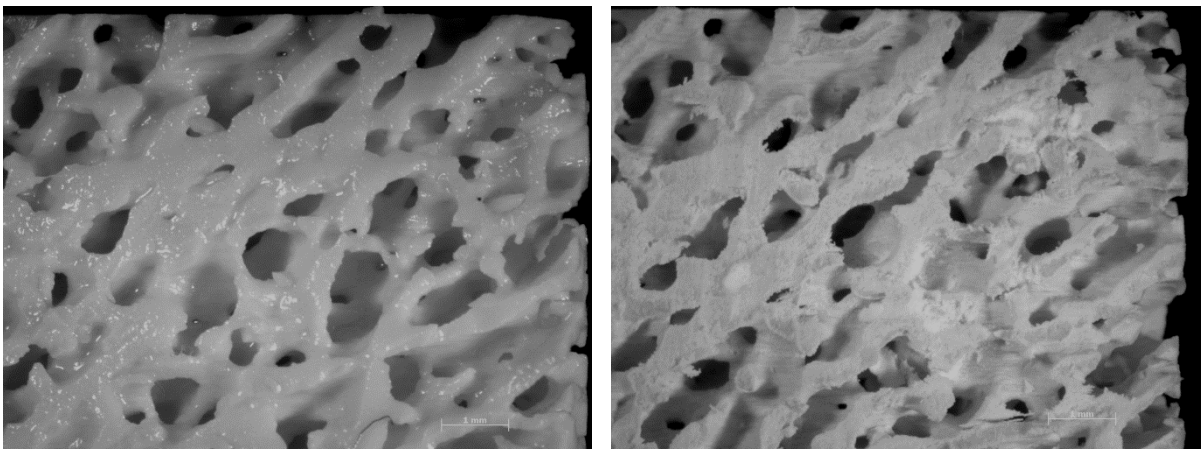

Figure 52. Light microscope images of the cross section of the manually cleaned parts with CS5 (left) and CS1 (right)

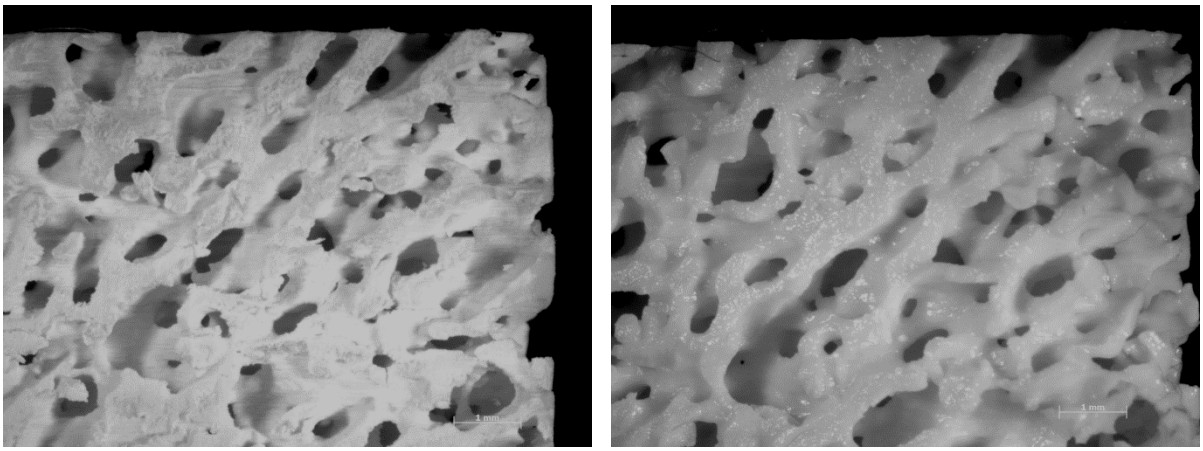

Figure 53. Light microscope images of the cross section of the manually cleaned parts with CS4 (left) and CS2 (right)

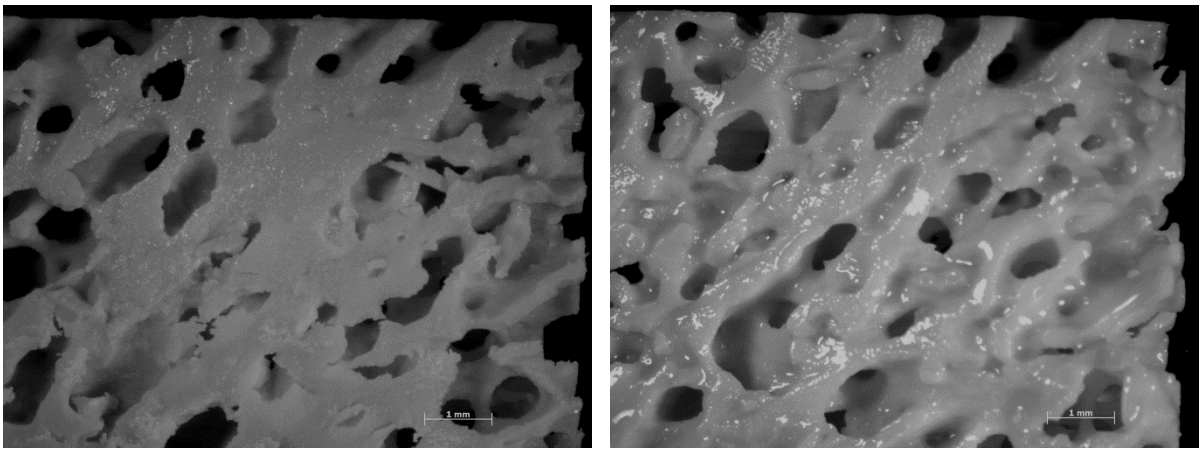

Figure 54. Light microscope images of the cross section of the manually cleaned parts with CS3 (left) and CS6 (right)

While manual cleaning can be efficient, it was noticed that some parts are not homogeneously cleaned, with some sections of the part still having residual slurry. It is therefore not convenient to clean the parts manually, as the repeatability of the process cannot be guaranteed. The results from the machine cleaning with solvent flowing from the top also show that all solvents are capable of cleaning the part (Figure 55, Figure 56 and Figure 57). All of the parts are cleaned thoroughly, which means that the method itself is effective.

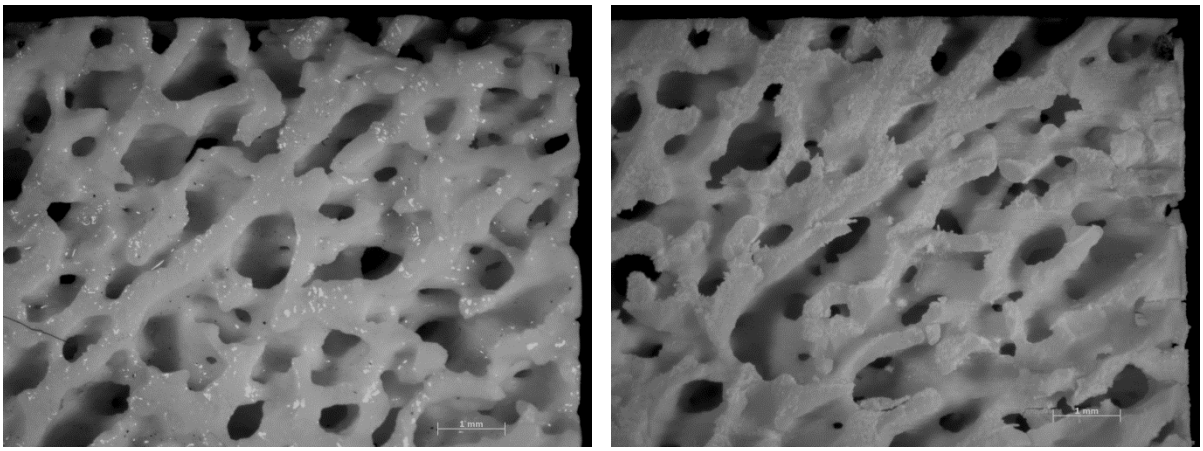

Figure 55. Light microscope images of the cross section of the machine cleaned parts (flow from top) with CS5 (left) and CS1 (right)

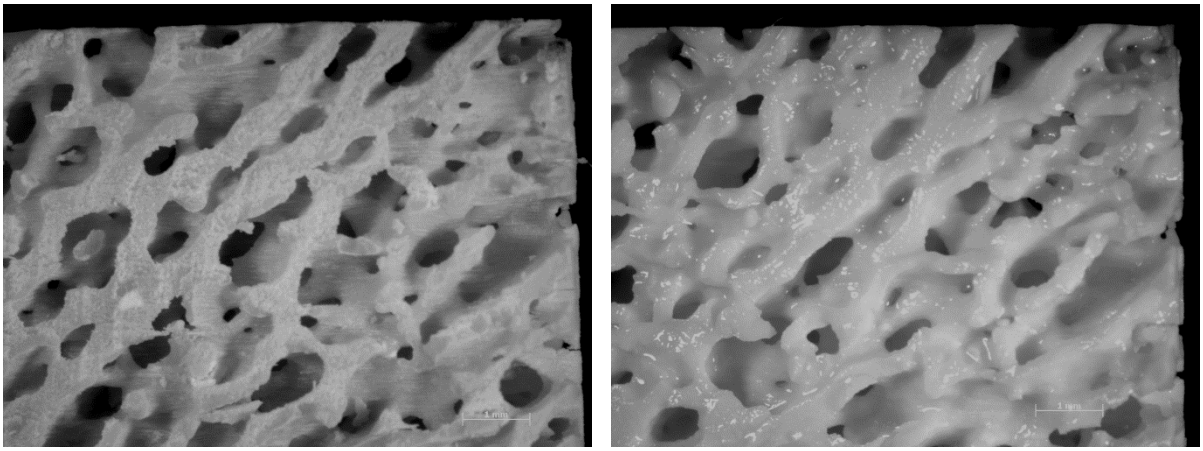

Figure 56. Light microscope images of the cross section of the machine cleaned parts (flow from top) with CS4 (left) and CS2 (right)

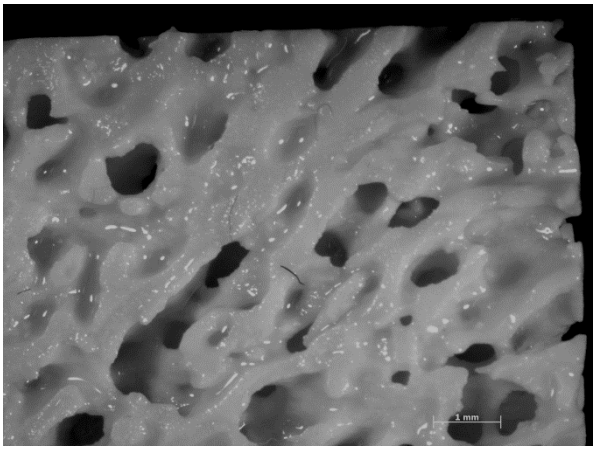

Figure 57. Light microscope image of the cross section of the machine cleaned part (flow from top) with CS6

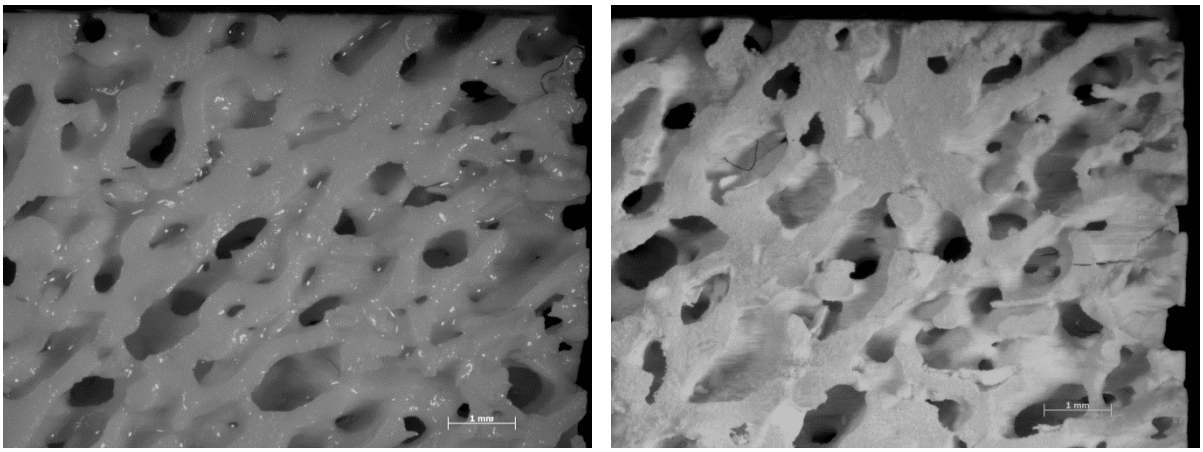

Figure 58. Light microscope images of the cross section of the machine cleaned parts (flow from top and bottom) with CS5 (left) and CS1 (right)

Machine cleaning with solvent flowing from top and bottom proved to be better than the manual cleaning, but not as efficient as the previous machine cleaning method (Figure 58).

Concerning solvents, it was determined earlier that CS3 is not an effective solution for the cleaning. The results of the swelling experiment show that CS6 and CS2 cause the most swelling of the green part (Table 5, Table 6 and Table 7). It was also noticed that parts cleaned with CS1 and CS4 are very fragile and easily destroyed during handling. CS5 caused the least swelling of the green part and ultimately, by comparing the images taken with SEM, it was concluded that it demonstrated the best cleaning performance (Figure 59 and Figure 60).

Table 5. Results of the swelling experiment for CS1 and CS3

Solvent	Dimension	0 h [mm]	24 h [mm]	Difference
CS1	h_1	2,97	2,97	0,00%
	h_2	1,96	1,97	0,51%
	h_3	0,99	0,99	0,00%
	h_4	0,49	0,49	0,00%
	l	29,76	29,54	-0,74%
CS3	h_1	2,95	2,97	0,68%
	h_2	1,97	1,97	0,00%
	h_3	0,99	0,99	0,00%
	h_4	0,5	0,49	-2,00%
	l	29,71	29,73	0,07%

Table 6. Results of the swelling experiment for CS2 and CS4

Solvent	Dimension	0 h [mm]	24 h [mm]	Difference
CS2	h_1	2,97	3,03	2,02%
	h_2	1,99	2,01	1,01%
	h_3	1,01	1,01	0,00%
	h_4	0,50	0,50	0,00%
	l	29,91	31,17	4,21%
CS4	h_1	2,96	2,96	0,00%
	h_2	1,97	1,97	0,00%
	h_3	1	0,99	-1,00%
	h_4	0,49	0,49	0,00%
	l	29,64	29,5	-0,47%

Table 7. Results of the swelling experiment for CS5 and CS6

Solvent	Dimension	0 h [mm]	24 h [mm]	Difference
CS5	h_1	2,97	2,97	0,00%
	h_2	1,97	1,97	0,00%
	h_3	1,00	1,00	0,00%
	h_4	0,49	0,49	0,00%
	l	29,85	30,02	0,57%
CS6	h_1	2,97	3,01	1,35%
	h_2	1,98	2,01	1,52%
	h_3	1,01	1,01	0,00%
	h_4	0,5	0,49	-2,00%
	l	29,8	30,8	3,36%

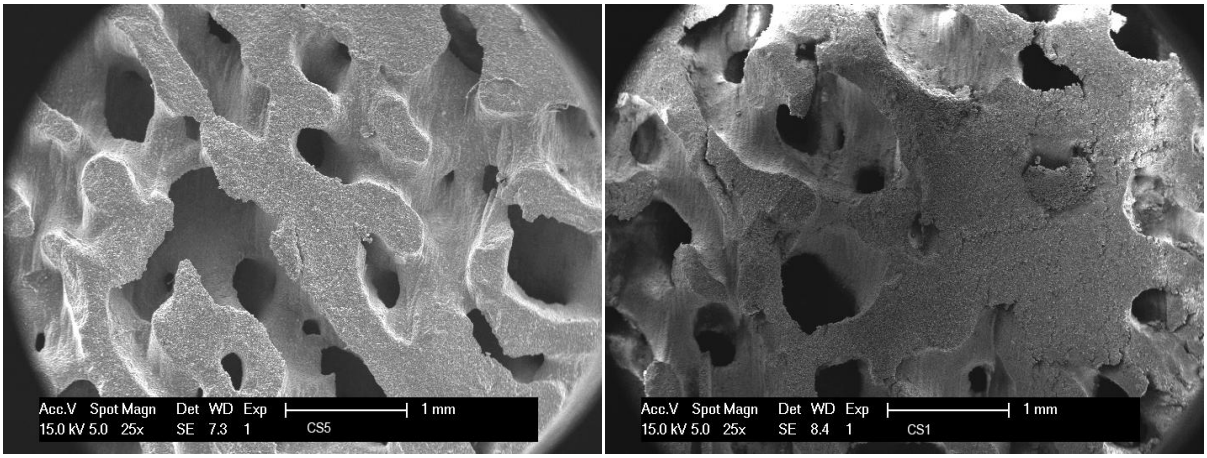

Figure 59. SEM images of the cross section of the machine cleaned parts (flow from top) with CS5 (left) and CS1 (right)

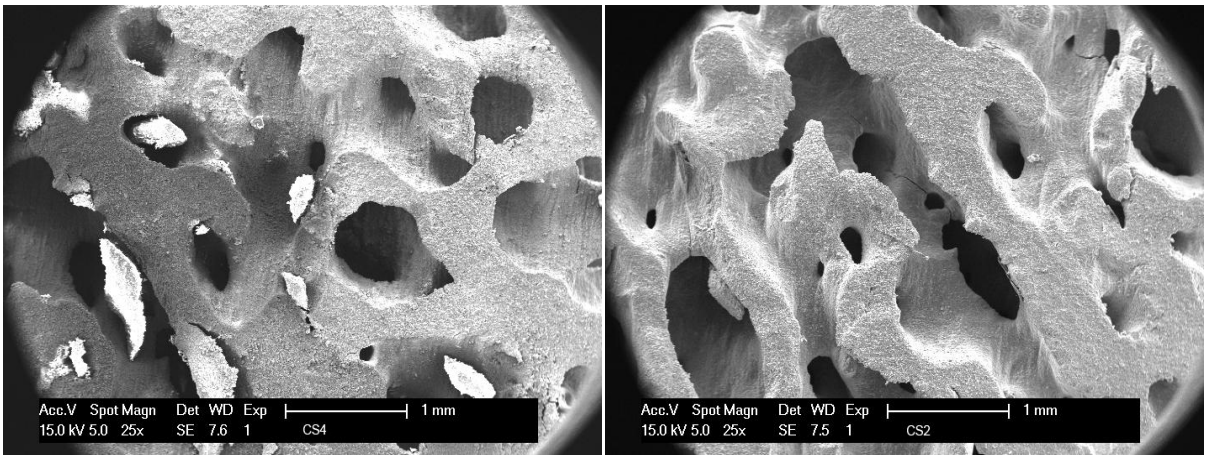

Figure 60. SEM images of the cross section of the machine cleaned parts (flow from top) with CS4 (left) and CS2 (right)

Therefore, the chosen method of cleaning is the machine cleaning with solvent flowing at a rate of 1,4 l/min from top, and the chosen solvent is CS5.

3.4. Thermal analysis

After adjusting the parameters according to the results of the TGA, an optimized heating programme was obtained (Figure 61). Compared to the initial programme, where the weight loss is very sharp, it can be seen that the optimized programme has a gradual weight loss. This way, formation of cracks inside the part can be avoided.

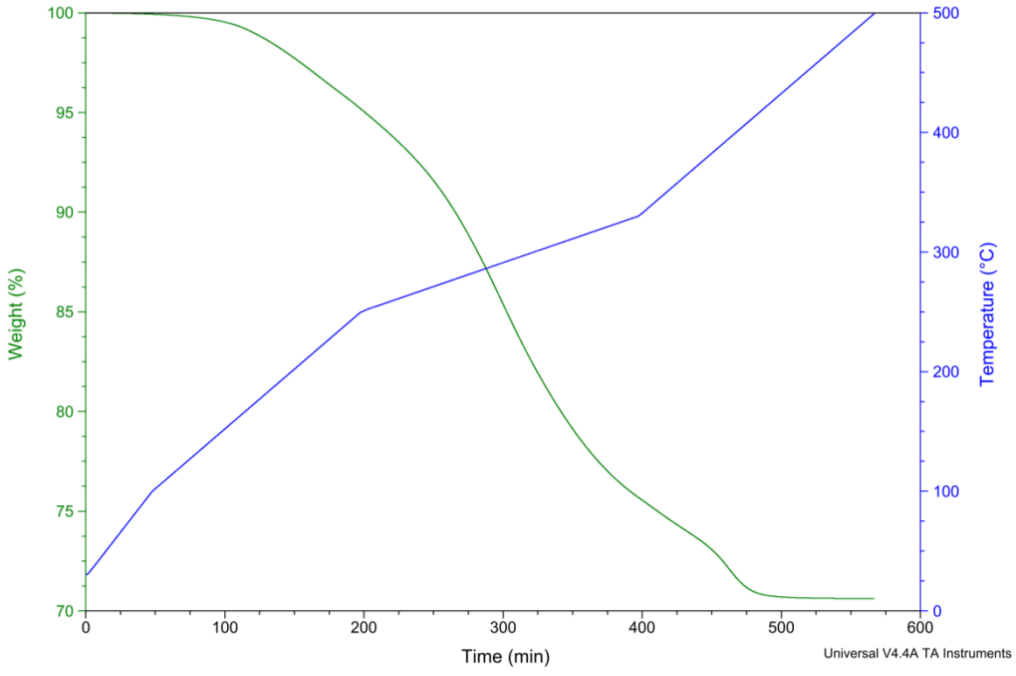

Figure 61. TGA measurement showing an approximately constant weight loss rate

However, TMA showed that the programme obtained from the TGA causes cracks in the part (Figure 62). Therefore, this programme was further adjusted until the final programme was obtained (Figure 63) which demonstrates that no cracks appeared.

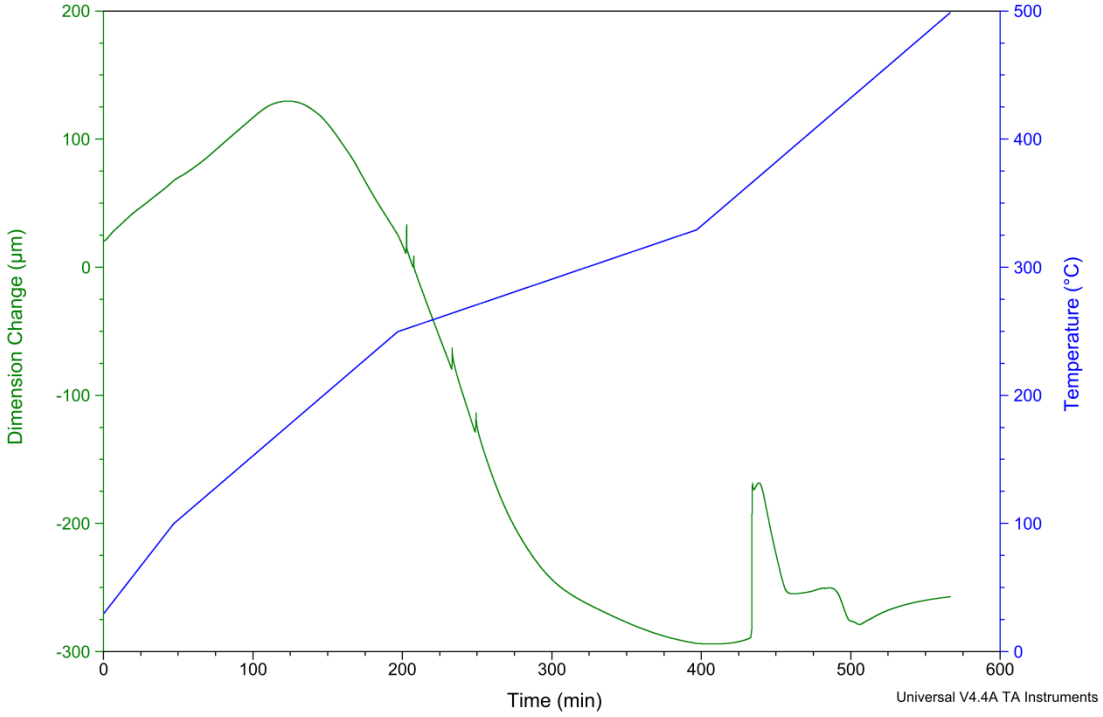

Figure 62. Initial TMA measurement

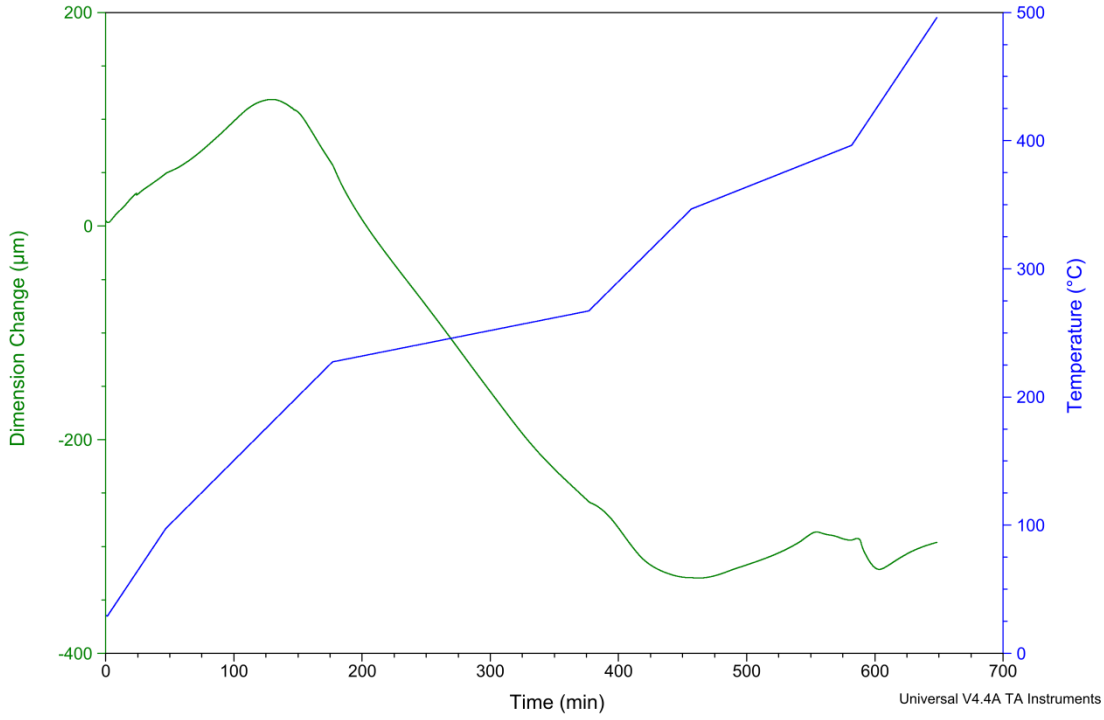

Figure 63. TMA measurement of the final heating programme

As mentioned previously, smaller parts are easier to debind than larger ones. After comparing Figure 62 and Figure 64, it is obvious that the dimension changes were less pronounced and fewer cracks appeared in the smaller cylinder, compared to the larger one, after using the same heating programme.

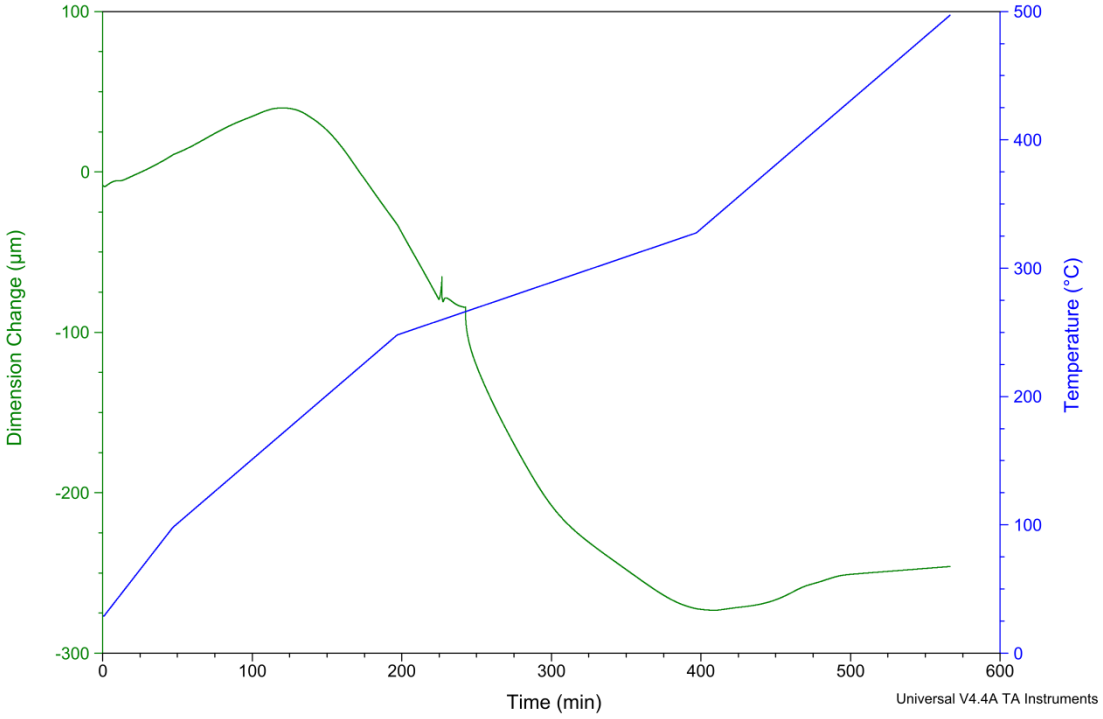

Figure 64. TMA measurement of the smaller diameter cylinder

With this analysis, an optimized heating programme was obtained. The new debinding programme takes less than 11 hours to complete, which is significantly faster compared to the programme used in [21], which takes 26 hours. It appears that no cracks appear during this process, although this still has to be tested.

4. SCAFFOLD DESIGN AND EVALUATION

Usage of computer-aided technologies in tissue engineering has evolved a development of a new field of Computer-Aided Tissue Engineering (CATE). CATE integrates advances in biology, biomedical engineering, information technology, and design and manufacturing to tissue engineering application [50]. Specifically, it applies computer-aided technologies, including computer-aided design (CAD), medical image processing, computer-aided manufacturing (CAM), and solid freeform fabrication (SFF) [50].

CATE design approach begins with the acquisition of non-invasive images and image processing of appropriate tissue region of interest [50]. This is followed by a 3D reconstruction of anatomical structure using commercially available medical reconstructive and reverse engineering software. The result of this step is a 3D CAD model of the defect site. Next, anatomic representative features are defined and a CAD model of a unit cell is generated. It is possible to design a customized heterogeneous tissue scaffold by adjusting unit cell properties. For instance, using different feature patterns to design a specific porous geometry, arranging feature patterns in a specific 3D architecture to form a preferable pore distribution and interconnectivity [51]. Afterwards, on the basis of the intended scaffold material, a finite element method is applied to determine the corresponding mechanical properties of the unit cell. Using CAD solid-modelling-based Boolean operations, the candidate unit cells can be integrated with the shape of the bone to form the bone tissue scaffold with specified internal architecture and structural properties (Figure 6) [50].

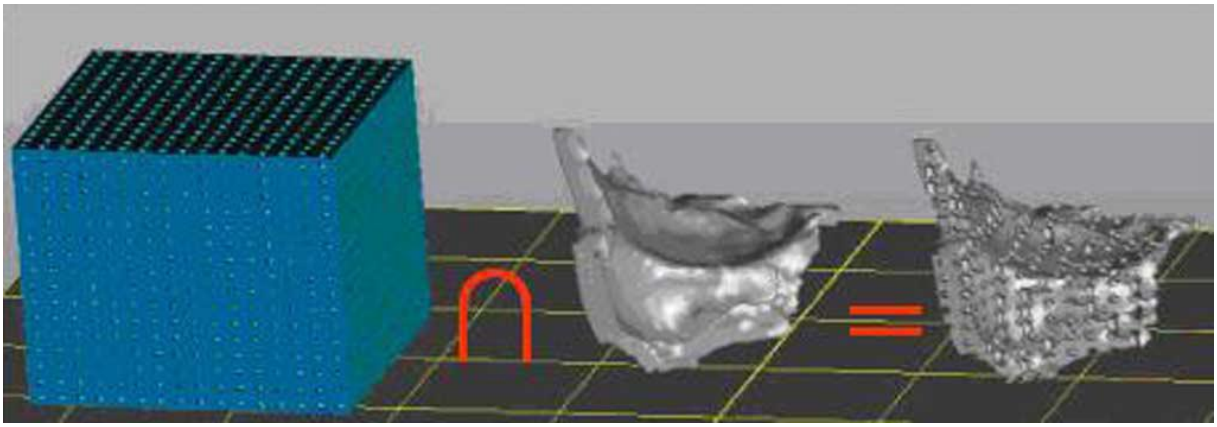

Figure 65. Example of using Boolean operation to achieve bone scaffold anatomical geometry [50]

As mentioned previously, tissue engineering for bone regeneration requires the use of a porous scaffold to serve as a template for cell interactions and the formation of the extracellular matrix, as well as to provide structural support for the newly formed tissue. These scaffolds should be able to withstand certain degree of loading during their use in vivo, besides providing the required biological response [52].

Within this thesis, a material was developed which enables printing of the complex structures, such as bone tissue scaffolds. Next step is to design the structures which can be used as a scaffold.

Before they are used, it is necessary to optimize their mechanical response so that they can provide the appropriate support while bone regenerates and they are slowly resorbed [52]. Predicting the mechanical behaviour of these complex 3D structures is therefore an essential task. Finite element method (FEM) has shown to be a tool that is capable of predicting the behaviour of complex structures, provided the mechanical properties of the materials comprising the structure are known.

Different parameters such as porosity, pore size, and interconnectivity of scaffolds influence the quality of tissue regeneration, among which porosity is the main design variable known to influence tissue regeneration [53]. Porosity of the ceramic scaffold has a great influence on the efficiency of bone tissue engineering as it directly influences cell adhesion, migration, and proliferation. Anatomically, cortical bone has 3%–12% porosity, while trabecular bone has porosity in the range of 50%–90% [3]. Since the primary target of bone tissue engineering is the regeneration of trabecular bone, porosity in the latter region should be ideal for ceramic scaffolds. Porosity is defined with the following equation:

$$\text{Porosity} = \left(1 - \frac{V_{scaffold}}{V_{total}}\right) \cdot 100\%, \tag{5}$$

where V_{scaffold} is the volume of scaffold geometry, while V_{total} is the overall volume enclosed by outer edges of the scaffold.

In this thesis, FEM was used to determine how the different geometrical variables and porosity can influence the mechanical behaviour of the structure. Two different scaffold structures were designed using Creo software (PTC Inc., USA). For each structure, two different porosity values were investigated (55% and 80%). Different porosities were achieved by varying the spacing between the rods and varying the size of the rods, therefore influencing the size of the pores. The analyzed scaffolds are shown in Figure 66, Figure 67, Figure 68 and Figure 69. The diameter of the circular rods for the 55% porosity and 80%

porosity scaffold is 0,5 mm and 0,35 mm respectively. The width and length of each scaffold is 6 mm, while height varies depending on the type of scaffold and its porosity, in the range of 3 – 6 mm. The dimensions of rectangular pores are 0,45x0,45 mm for the 55% porosity, and 0,65x0,65 mm for the 80% porosity scaffold.

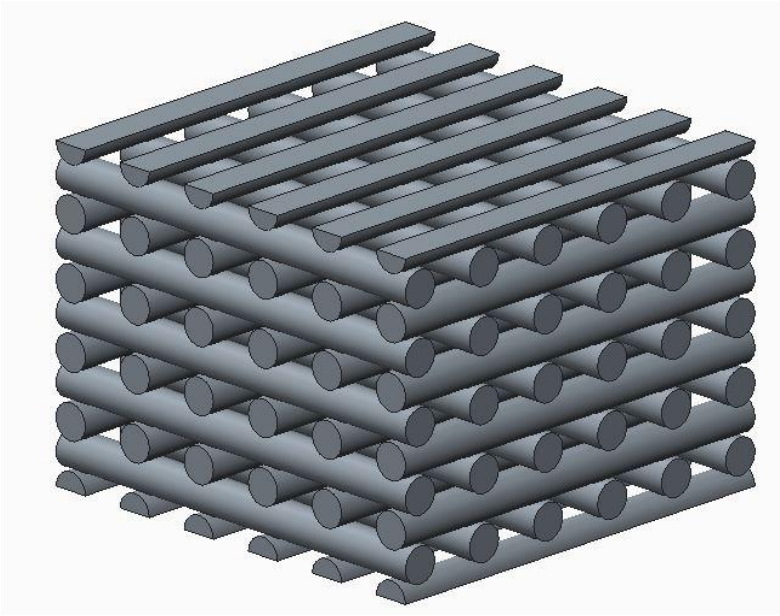

Figure 66. Scaffold with circular rods and a porosity of 55%

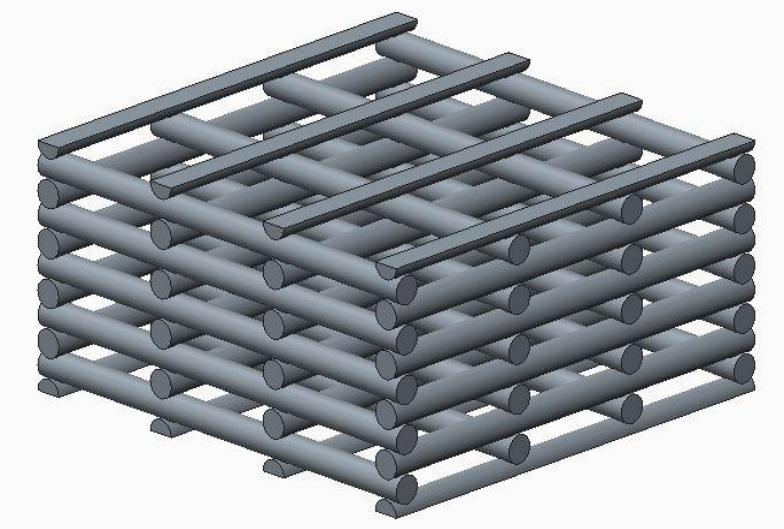

Figure 67. Scaffold with circular rods and a porosity of 80%

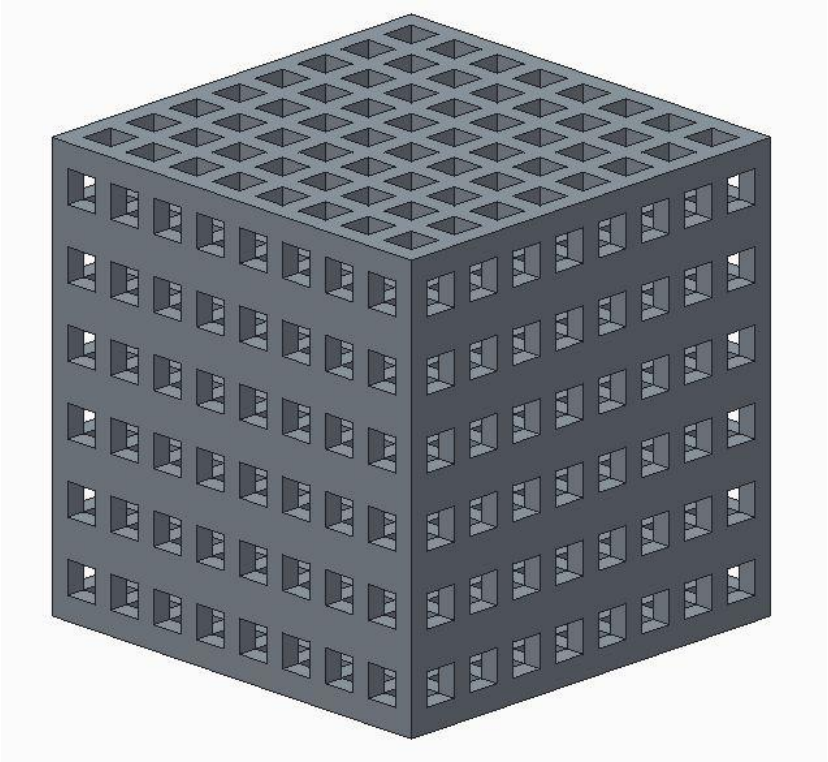

Figure 68. Scaffold with rectangular pores and 55% porosity

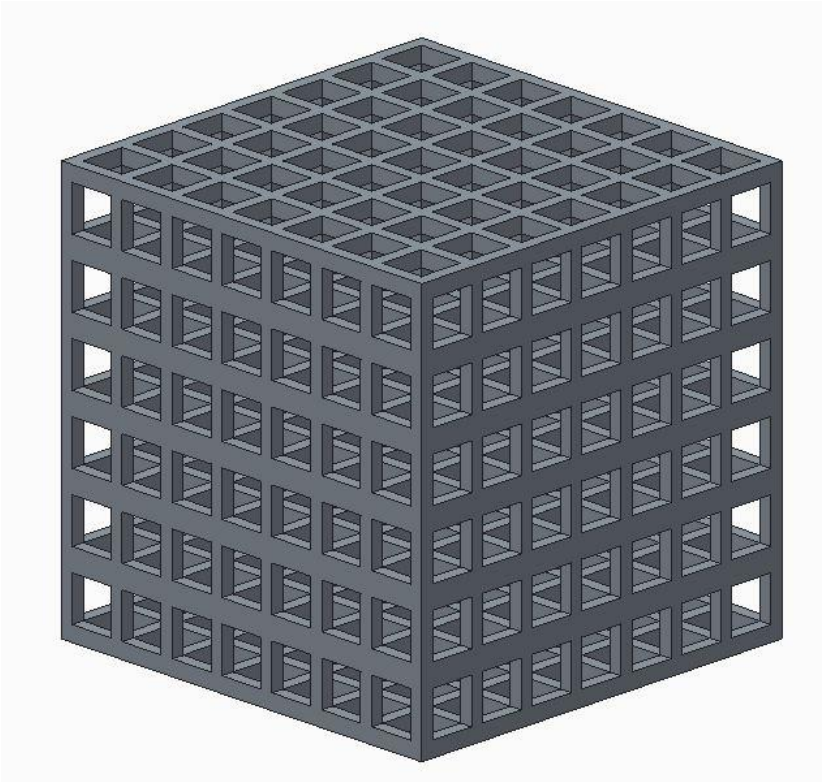

Figure 69. Scaffold with rectangular pores and 80% porosity

As determined in the experiments which were not part of this thesis, Young's modulus of 98 MPa and Poisson's ratio of 0,28 [52] were used as the mechanical properties of the sintered TCP. The mesh was generated, and the stress was analyzed using the Abaqus software (Dassault Systèmes, France). The equivalent von Mises stress was evaluated for all of the 4 designed structures. Each structure was meshed with a different number of tetrahedral elements, and the values can be seen in Table 3.

Table 8. Number of finite elements for each scaffold

Type of scaffold	Porosity	Number of elements
Circular rods	55 %	396019
	80 %	99095
Rectangular pores	55 %	243239
	80 %	123138

In order to simulate the compression of the scaffold, and according to [51, 54], a displacement of 0,5% of the scaffold height was applied at the top surface. The bottom surface was constrained in all three directions of space.

The undeformed and deformed shapes of both types of scaffold with 55% porosity are shown in Figure 70 and Figure 71. The resulting von Mises stress distributions can be seen in Figure 72, Figure 73, Figure 75 and Figure 76.

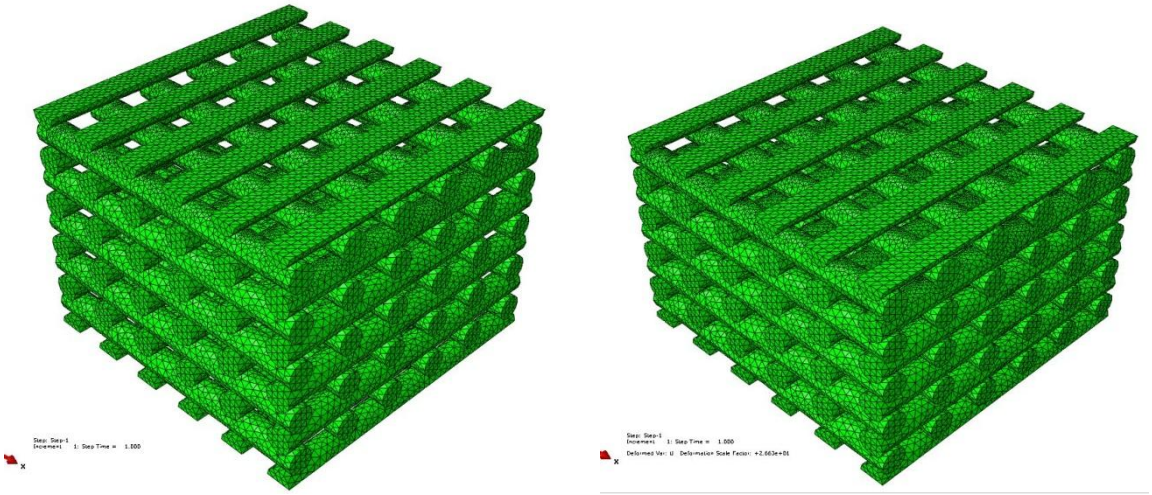

Figure 70. Undeformed (left) and deformed (right) shape of the circular rods scaffold with 55% porosity

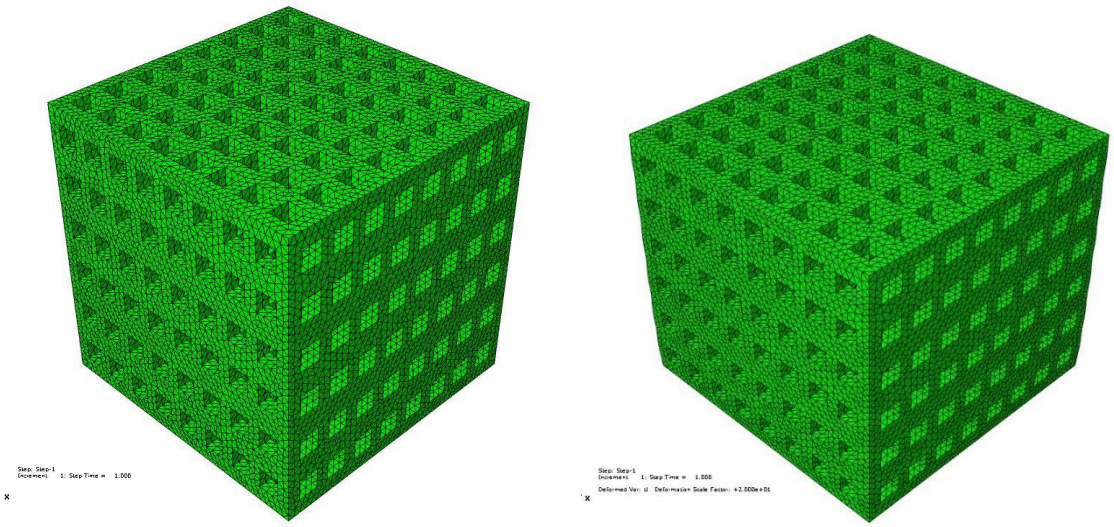

Figure 71. Undeformed (left) and deformed (right) shape of the rectangular pores scaffold with 55% porosity

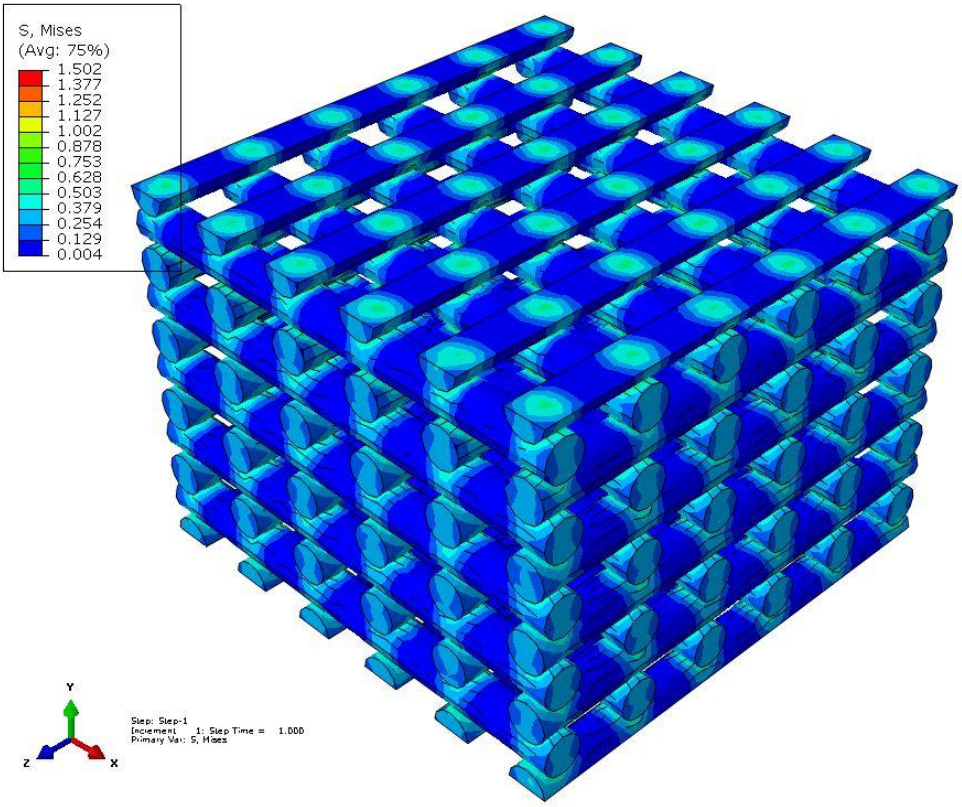

Figure 72. Von Mises stress distribution (in MPa) in the circular rod scaffold with 55% porosity

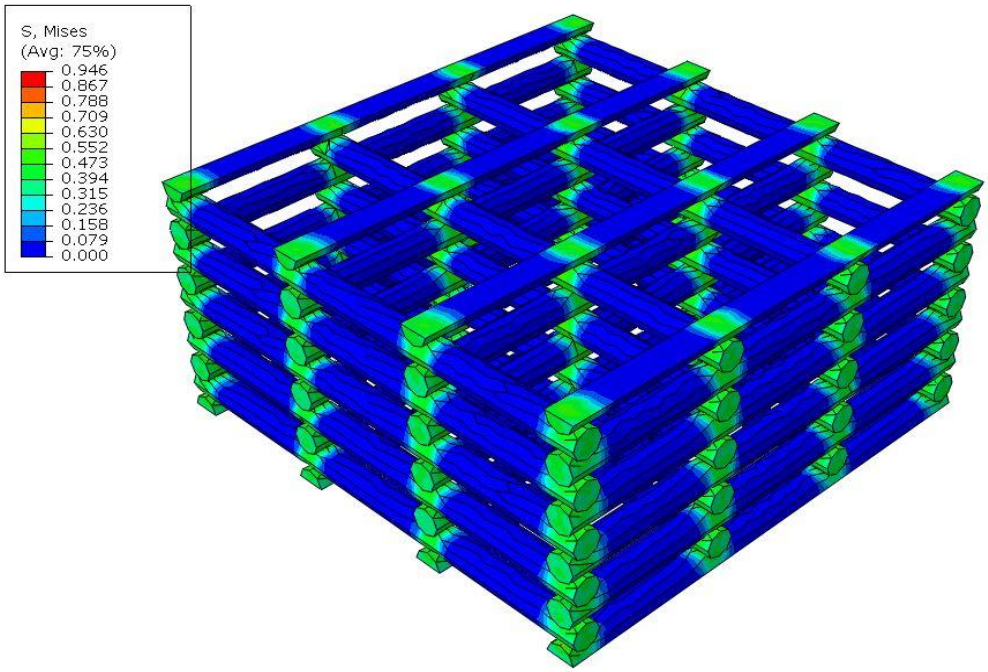

Figure 73. Von Mises stress distribution (in MPa) in the circular rod scaffold with 80% porosity

Highest stress values for all of the scaffolds are shown in Table 9. From the results shown in Figure 72, Figure 73 and Figure 74, it can be seen that the highest stress occurs on the contact of the rods. Although the stress values appear to be similar in both the 55% porosity and 80% porosity scaffold, the stress is more evenly distributed in the lower porosity scaffold. In the higher porosity scaffold, the stress is more pronounced on the vertical line which connects the contact points of the rods. It means that a perpendicular rod clamped between two parallel rods is under higher stress compared to the same rod in the lower porosity scaffold. This can be caused by a smaller diameter of the rods in the higher porosity scaffold, as this smaller diameter can create stress concentration points in the adjacent rod.

Table 9. Highest stress values

Type of scaffold	Porosity	Von Mises stress [MPa]
Circular rods	55 %	1,502
	80 %	0,946
Rectangular pores	55 %	0,910
	80 %	0,879

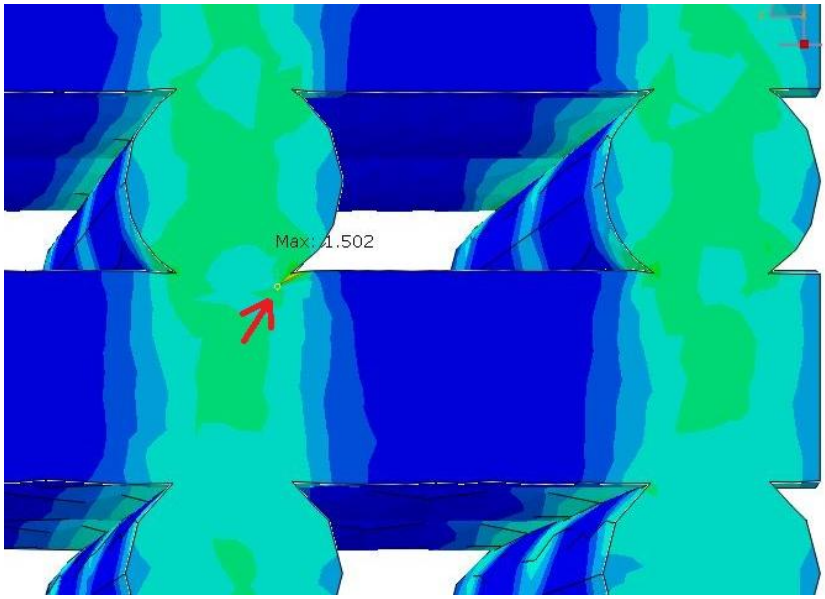

Figure 74. Location of the highest stress in the circular rod scaffold with 55% porosity

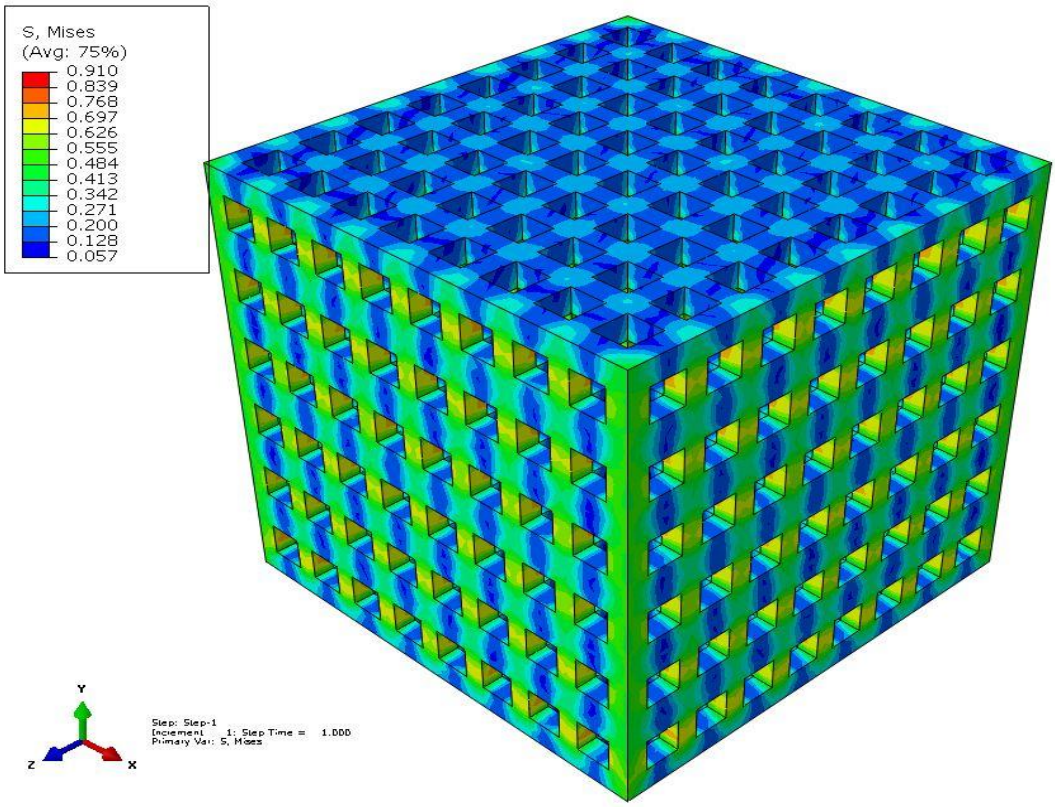

Figure 75. Von Mises stress distribution (in MPa) in the rectangular pore scaffold with 55% porosity

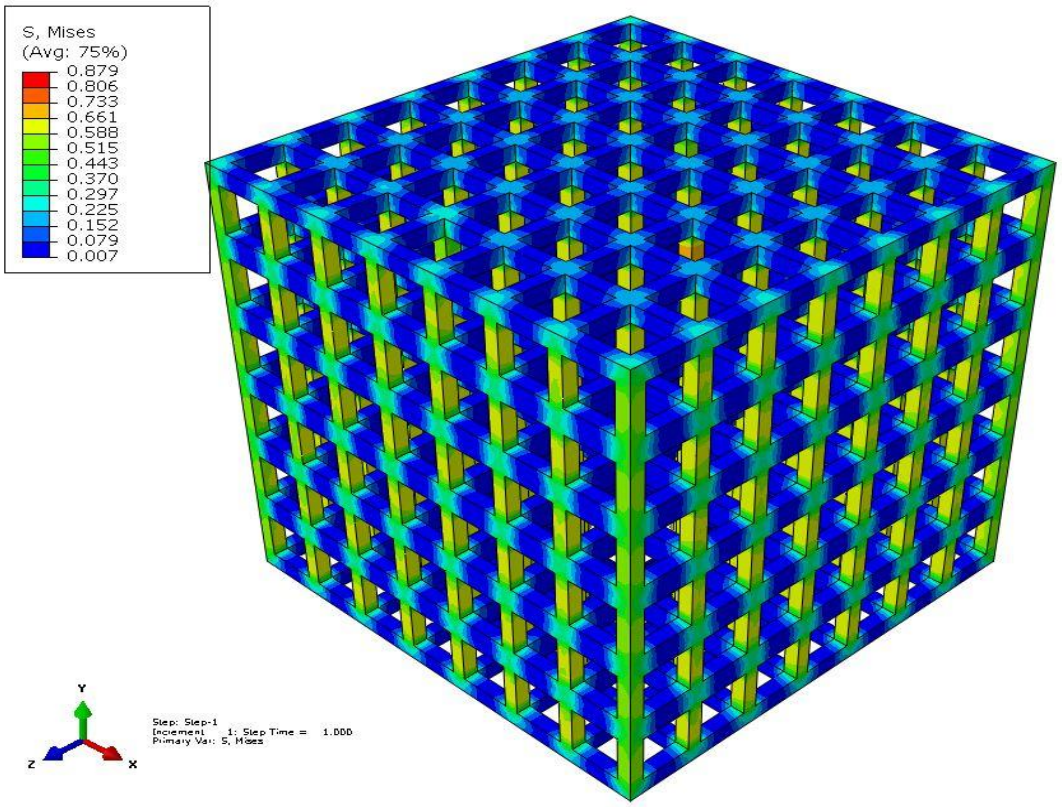

Figure 76. Von Mises stress distribution (in MPa) in the rectangular pore scaffold with 80% porosity

Figure 75 and Figure 76 show that in this type of scaffold, stress remains almost the same with the increase in scaffold porosity. However, in both cases, the sharp edges of the pores can cause stress concentration which could affect the mechanical stability of the scaffold (Figure 77). Furthermore, thin vertical walls of the pores have higher stress compared to the rest of the structure. As with the previous scaffold design, lower porosity scaffold provides more even stress distribution.

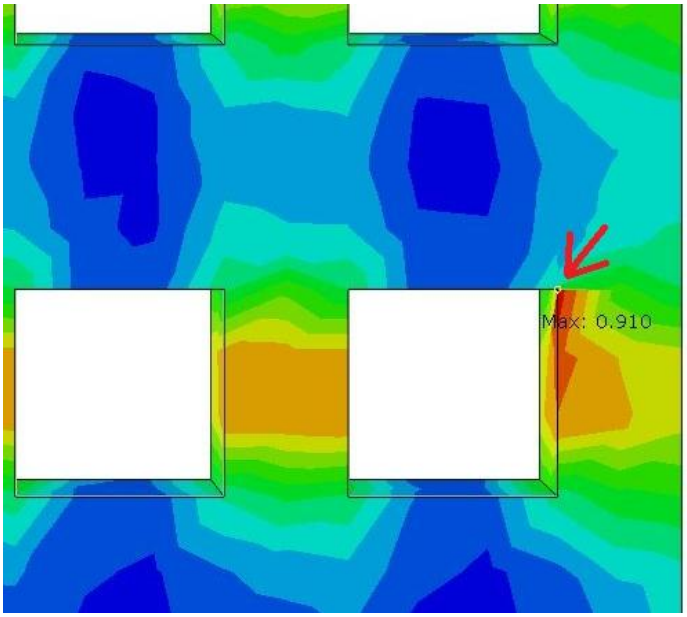

Figure 77. Location of the highest stress in the rectangular pore scaffold with 55% porosity

5. CONCLUSION

From all the carried out experiments, several conclusions can be drawn. However, a few notes have to be taken into account. The comparison of the printing quality was done based on only one printed sample. Therefore, it is possible that in second or third try, the printing quality of a slurry could be different. The rheology measurements were also carried out only once for each slurry, which was previously used on the Blueprinter, therefore the real values could differ from the ones obtained in this thesis. Also, the proposed thermal treatment needs to be further tested to conclude if it is definitely suitable for the new slurry. It is a general guidance for the newly developed slurry, but it needs to be adjusted according to the specific shape which will be fabricated.

Conclusions drawn during creation of this thesis:

- The addition of wax significantly improves the stability of the slurry and decreases the printing quality, while keeping the viscosity at the same value. Therefore, by carefully adjusting the wax content, it was possible to achieve a stable slurry with required printing quality.
- Usage of higher molecular weight solvents improves the stability and it can negatively influence the printing quality. It was determined that the lower molecular weight solvent is more suitable as it allows the required printing quality to be achieved.
- Compatibility between components is an important factor which can have an effect on the stability of the slurry. It can also influence layer to layer adhesion during printing, therefore influencing the printing quality. In order to obtain better compatibility, it is better to use monomers of the same type: acrylates or methacrylates. It is also beneficial to use wax-monomer combinations which are compatible regarding their polarity.
- Higher solid loading improves the stability, increases the viscosity and decreases the printing quality. An appropriate value of solid loading was determined, which provides improved stability, while maintaining the required printing quality.
- Increasing the monomer content improves the printing quality and decreases the stability of the slurry. By adjusting the monomer content, and with the addition of wax, it was possible to improve printing quality while maintaining the slurry stability.

- Dispersing agents can significantly influence viscosity of the slurry, therefore influencing the stability. An appropriate dispersing agent was determined, which provides good stability and printing quality.
- Increasing the light absorber content improves the printing quality of smaller details, but over a certain value no further improvement is possible. Increasing the light absorber content also increases the energy needed for the curing, which can cause overgrowing of the part. Therefore, the appropriate light absorber content was determined, which improves the printing quality and causes the least overgrowing of the part.
- Increasing the photoinitiator content decreases the energy needed for the successful curing. An increased photoinitiator content was determined as the optimum, as it provides the printing to be carried out with lower light intensity, while maintaining the required printing quality.

In this thesis, a stable slurry with increased solid loading was achieved, which enables printing with improved quality. Furthermore, an appropriate cleaning procedure for the green part was determined. Also, the thermal treatment was optimized in order to obtain a dense ceramic part.

In the second part of the thesis, FEM was used to determine how the different geometrical variables and porosity can influence the mechanical behaviour of the structure. Based on the obtained results, it can be concluded that scaffold with circular rods and lower porosity provides favourable stress distribution, while the rectangular pore scaffold allows the use of higher porosity. In general, when designing scaffolds, it is necessary to make a compromise between the mechanical behaviour of the scaffold and its overall porosity.

REFERENCES

[1] O'Brien, F.J.: *Biomaterials and scaffolds for tissue engineering*, Trinity Centre for Bioengineering, Department of Mechanical Engineering, Trinity College Dublin, Ireland, 2011.

[2] Moroni, L.: *A Mechanistic Approach to Design Smart Scaffolds for Tissue Engineering*, PhD Thesis, University of Twente, Enschede, The Netherlands, 2006.

[3] Khang, G.: *Handbook of Intelligent Scaffolds for Tissue Engineering and Regenerative Medicine*, Pan Stanford, USA, 2012.

[4] Zilbermann, M.:, *Active Implants and Scaffolds for Tissue Regeneration*, Springer, 2011.

[5] Khang, G., Kim, M.S., Lee, H.B.: *A manual for biomaterials/scaffold fabrication technology*, World Scientific Publishing, Singapore, 2007.

[6] Qin, L., Genant, H.K., Griffith, J.F., Leung, K.S.: *Advanced Bioimaging Technologies in Assessment of the Quality of Bone and Scaffold Materials*, Springer, 2007.

[7] Laurencin, C.T., Nair, L.S.: *Nanotechnology and Tissue Engineering -The Scaffold*, CRC Press, USA, 2008.

[8] Liebschner, M.A.K.: *Computer-Aided Tissue Engineering*, Humana Press, USA, 2012.

[9] Sharma, C.P.: *Biointegration of medical implant materials*, Woodhead Publishing, UK, 2010.

[10] Zhang, L.G., Fisher, J.P., Leong, K.W.: *3D Bioprinting and Nanotechnology in Tissue Engineering and Regenerative Medicine*, Elsevier, 2015.

[11] Fisher, J.P., Mikos, A.G., Bronzino, J.D.: *Tissue Engineering*, CRC Press, USA, 2007.

[12] Sultana, N.: *Biodegradable Polymer-Based Scaffolds for Bone Tissue Engineering*, Springer, 2013.

[13] Sakka, S., Bouaziz, J., Ben Ayed, F.: *Mechanical Properties of Biomaterials Based on Calcium Phosphates and Bioinert Oxides for Applications in Biomedicine*, Sfax University, Tunisia, 2013.

[14] Billotte, W. G.: *Ceramic Biomaterials*, CRC Press, USA, 2000.

[15] Izadifar, Z., Chen, X., Kulyk, W.: *Strategic Design and Fabrication of Engineered Scaffolds for Articular Cartilage Repair*, J. Funct. Biomater., 2012.

[16] Gross, B.C., Erkal, J.L., Lockwood, S.Y., Chen, C., and Spence, D.M.: *Evaluation of 3D Printing and Its Potential Impact on Biotechnology and the Chemical Sciences*, Analytical Chemistry, USA, 2014.

[17] Griffith, M.L., Halloran, J.W.: *Free Form Fabrication of Ceramics By Stereolithography*, J. American Ceramic Soc., USA, 1994.

[18] Honiball, J.R.: *The Application of 3D Printing in reconstructive surgery*, Dissertation, University of Stellenbosch, South Africa, 2010.

[19] Bartolo, P.J.: *Stereolithography*, Springer, 2011.

[20] Lee, J.H., Prud'homme, R.K., Aksay, I.A.: *Cure depth in photopolymerization*, Princeton University, USA, 2001.

[21] Mitteramskogler, G.: *Generative Fertigung von Bauteilen aus TCP*, Diplomarbeit, Vienna University of Technology, Austria, 2011.

[22] Felzmann, R., Gruber, S., Mitteramskogler, G., Tessavibul, P., Boccaccini, A.R., Liska, R., Stampfl, J.: *Lithography-Based Additive Manufacturing of Cellular Ceramic Structures*, Advanced Engineering Materials, 2012.

[23] Pfaffinger, M., Mitteramskogler, G., Gmeiner, R., Stampfl, J.: *Thermal debinding of ceramic-filled photopolymers*, Vienna University of Technology, Austria, 2015.

[24] Fouassier, J.P., Lalevée, J.: *Photoinitiators for Polymer Synthesis*, Wiley-VCH, 2013.

[25] Orthaber, U.: *Photopolymerization*, University of Ljubljana, 2010.

[26] *Photopolymerization*, http://web.itu.edu.tr/~yusuf/index-1.htm

[27] Moszner, N.: *Photopolymerization in dentistry*, Ivoclar Vivadent Report, 2013.

[28] Gmeiner, R., Mitteramskogler, G. Stampfl, J.: *Stereolithographic Ceramic Manufacturing of High Strength Bioactive Glass*, Int. J. Appl. Ceram. Technol., 2014.

[29] Mitteramskogler, G., Gmeiner, R., Felzmann, Gruber, S., Hofstetter, C., Stampfl, J., Ebert, J., Wachter, W., Laubersheimer, J.: *Light curing strategies for lithography-based additive manufacturing of customized ceramics*, Elsevier, 2014.

[30] Hinczewski, C., Corbel, S., Chartie, T.: *Ceramic Suspensions Suitable for Stereolithography*, Journal of the European Ceramic Society, 1998.

[31] Conley, R.F.: *Practical Dispersion – A Guide to Understanding and Formulating Slurries*, Wiley-VCH, USA, 1996.

[32] *Cationic Photoinitiators*, https://www.sigmaaldrich.com/content/dam/sigma-aldrich/docs/Aldrich/Technical_Ads/al_ms_ad7_photoinitiators.pdf

[33] Zheng, X.: *Design and optimization of a light-emitting diode projection micro stereolithography three-dimensional manufacturing system*, American Institute of Physics, USA, 2012.

[34] *Colloidal dispersions*, http://www.chemistrylearning.com/colloidal-dispersions/, 31.5.2016.

[35] *Colloidal solution*, http://www.chemistrylearning.com/colloidal-solution-true-solution-and-suspension/, 31.5.2016.

[36] *Suspensions*, http://www.edinformatics.com/math_science/suspensions_colloids.htm, 31.5.2016.

[37] Shi, J.:*Steric Stabilization*, The Ohio State University, USA, 2002.

[38] *Colloid*, https://en.wikipedia.org/wiki/Colloid, 31.5.2016.

[39] De Blas Romero, A.: *Optimization of photocurable zirconia slurries*, Master thesis, Vienna University of Technology, Austria, 2014.

[40] Mewis, J., Wagner, N.J.: *Colloidal Suspension Rheology*, Cambridge University Press, UK, 2012.

[41] *Colloidal suspensions*, http://physics.gu.se/~frtbm/joomla/media/mydocs/LennartSjogren/kap9.pdf, 30.5.2016.

[42] *Stabilization of Aqueous Ceramic Powder Suspensions*, http://besyo.mu.edu.tr/icerik/metalurji.mu.edu.tr/Sayfa/Stabilization%20of%20Aqueous%20Ceramic%20Powder%20Suspensions.pdf

[43] *Monomers*, http://www.che.hw.ac.uk/teaching/B11MS1/Material/BackgroundMaterial/Monomers.htm, 8.6.2016.

[44] *Monomer functionality*, http://goldbook.iupac.org/FT07505.html

[45] *Polyacrylates*, http://pslc.ws/macrog/acrylate.htm

[46] Fontanille, M., Guyot, A.: *Recent Advances in Mechanistic and Synthetic Aspects of Polymerization*, D. Reidel Publishing Company, Holland, 1987.

[47] *Radical stability*, http://chemwiki.ucdavis.edu/Textbook_Maps/Organic_Chemistry_Textbook_Maps/Map%3A_Organic_Chemistry_(Bruice)/12%3A_Radicals_(Reactions_of_Alkanes)/12.03%3A_Radical_Stability_Depends_on_the_Number_of_Alkyl_Groups_Attached_to_the_Carbon_with_the_Unpaired_Electron

[48] *Thermogravimetric analysis*, http://www.andersonmaterials.com/tga.html

[49] *Thermomechanical analysis*, https://www.netzsch-thermal-analysis.com/en/products-solutions/thermomechanical-analysis/

[50] Sun, W., Starly, B., Nam, J., Darling, A.: *Bio-CAD modeling and its applications in computer-aided tissue engineering*, Computer-Aided Design, Elsevier, 2005.

[51] Starly, B.: *Biomimetic design and fabrication of tissue engineered scaffolds using computer aided tissue engineering*, PhD Thesis, USA, 2006.

[52] Miranda P., Pajares, A., Guiberteau, F.: *Finite element modeling as a tool for predicting the fracture behavior of robocast scaffolds*, Elsevier, 2008.

[53] Entezari, A., Zhang, Z., Chen, J., Li, Q.: *Optimization of bone tissue scaffolds fabricated by robocasting technique*, 11thWorld Congress on Structural and Multidisciplinary Optimisation, Australia, 2015.

[54] Podshivalov, L., Gomes, C.M., Zocca, A., Guenster, J., Bar-Yoseph, P., Fischer, A.: *Design, analysis and additive manufacturing of porous structures for biocompatible micro-scale scaffolds*, Elsevier, 2013.

APPENDIX

I. CD-R disc